

# **Robust Haptics with Nonlinear Impedance Matching for Robot-assisted Laparoscopic Surgery**

**Mohammad Mazidi**

**A Thesis**

**in**

**The Department**

**of**

**Mechanical, Industrial, and Aerospace Engineering**

**Presented in Partial Fulfillment of the Requirements**

**for the Degree of**

**Master of Applied Science (Mechanical Engineering) at**

**Concordia University**

**Montréal, Québec, Canada**

**January 2025**

**© Mohammad Mazidi, 2025**

CONCORDIA UNIVERSITY

School of Graduate Studies

This is to certify that the thesis prepared

By: **Mohammad Mazidi**

Entitled: **Robust Haptics with Nonlinear Impedance Matching for Robot-assisted  
Laparoscopic Surgery**

and submitted in partial fulfillment of the requirements for the degree of

**Master of Applied Science (Mechanical Engineering)**

complies with the regulations of this University and meets the accepted standards with respect to originality and quality.

Signed by the Final Examining Committee:

\_\_\_\_\_ Chair  
*Dr. Youmin Zhang*

\_\_\_\_\_ Examiner  
*Dr. Youmin Zhang*

\_\_\_\_\_ Examiner  
*Dr. Hang Xu*

\_\_\_\_\_ Supervisor  
*Dr. Javad Dargahi*

\_\_\_\_\_ Co-supervisor  
*Dr. Amir Hooshidar*

Approved by \_\_\_\_\_  
Muthukumaran Packirisamy, Chair  
Department of Mechanical, Industrial, and Aerospace Engineering

\_\_\_\_\_ 2025

\_\_\_\_\_  
Mourad Debbabi, Dean  
Faculty of Engineering and Computer Science

# Abstract

## Robust Haptics with Nonlinear Impedance Matching for Robot-assisted Laparoscopic Surgery

Mohammad Mazidi

The integration of haptic feedback into robot-assisted minimally invasive surgery (RAMIS) has been constrained by challenges in accurately rendering forces while maintaining system stability and safety. Addressing these limitations, this research introduces the Nonlinear Impedance Matching Approach (NIMA), a novel force-rendering method designed to accurately model complex tool-tissue interactions. Building on the Impedance Matching Approach (IMA), NIMA incorporates nonlinear dynamics to enhance the precision and reliability of force feedback systems.

The experimental results demonstrate that NIMA achieves a mean absolute error (MAE) of  $0.01 \pm 0.02$  N, representing a 95% reduction in error compared to IMA. Notably, NIMA eliminates haptic "kickback" by ensuring that no residual force is applied to the user's hand when releasing the haptic device, significantly improving both user comfort and patient safety. Furthermore, its ability to account for the nonlinearities of tool-tissue interactions allows for high fidelity, responsiveness, and precision across diverse surgical conditions.

This research advances the development of robust, high-performance haptic systems, offering a transformative solution to the challenges of force rendering in teleoperated surgical robotics. By providing a realistic and reliable interface for robotic-assisted surgical procedures, NIMA has the potential to enhance surgical precision, optimize patient outcomes, and set new standards for haptic feedback in RAMIS.

# Acknowledgments

This thesis marks the culmination of years of hard work, perseverance, and personal growth, and it would not have been possible without the support, guidance, and love of so many wonderful people. It is with a profound sense of gratitude that I take this opportunity to acknowledge and thank them.

First and foremost, my deepest and most heartfelt thanks go to my parents. Your unwavering love, selflessness, and sacrifices have been my guiding light throughout my life. You have been my greatest teachers, instilling in me the values of resilience, curiosity, and determination. Your faith in my abilities, even during my moments of doubt, has been my anchor and my source of strength. I owe every step of my success to your constant encouragement and unconditional support.

To my sisters and my brother, thank you for being my pillars of strength and understanding. Your endless care, advice, and camaraderie have always given me the motivation to strive for my best. You have celebrated my victories as your own and provided me comfort during my challenges, for which I am forever grateful.

I would also like to express my gratitude to my incredible friends, who have been my emotional sanctuary throughout this journey. Navid and Kimia, your unwavering belief in me and your constant encouragement made even the hardest days bearable. Whether it was through late-night conversations, shared laughter, or simply being there when I needed it most, your friendship has been a source of immense strength and joy. To my broader circle of friends, thank you for your kind words, your patience, and your support. You all have played an irreplaceable role in this journey.

A special mention goes to Dr. Amir Hooshier and Dr. Javad Dargahi, my supervisors, whose invaluable guidance, mentorship, and encouragement have been instrumental in shaping both this

thesis and my academic journey. Your expertise and insightful advice have been a cornerstone of this work, and I am deeply grateful for the opportunity to learn and grow under your supervision.

I would also like to thank the Examining Committee for their time, effort, and constructive feedback during the evaluation of this thesis. Your insights and suggestions have helped refine and improve this work, and I sincerely appreciate your contributions.

A special note of gratitude goes to Nima, whose expertise and willingness to assist in the integration of the setup used in this thesis were invaluable. Your collaboration and insights significantly contributed to the success of this project, and I cannot thank you enough for your generosity and dedication.

I am also deeply indebted to Erfan, whose remarkable contributions in designing the adaptors, calibrating, and integrating the setup used in this thesis were nothing short of extraordinary. Your technical skills, patience, and commitment have left an indelible mark on this work, and I feel privileged to have had your support throughout this process.

Finally, I want to acknowledge everyone who has played a role in this journey, however big or small. Your kindness, encouragement, and belief in me have carried me through the most challenging times, and I am endlessly grateful for the role you've played in my life.

This thesis is as much a testament to your love and support as it is to my hard work. I dedicate this achievement to all of you.

# Contents

<b>List of Figures</b>	<b>viii</b>
<b>List of Tables</b>	<b>xi</b>
<b>1 Introduction</b>	<b>1</b>
1.1 Background . . . . .	1
1.1.1 Minimally Invasive Surgery (MIS) . . . . .	1
1.1.2 Robot Assisted Laparoscopic surgery . . . . .	2
1.1.3 Clinical Need for Force Feedback in Robot-assisted Laparoscopic Surgery . . . . .	4
1.2 Research Objectives . . . . .	6
1.3 Publications . . . . .	7
1.4 Thesis layout . . . . .	8
<b>2 Nonlinear Impedance Matching Approach (NIMA) for Robust Haptic Rendering during Robotic Laparoscopy Surgery</b>	<b>10</b>
2.1 Objective and Contributions . . . . .	10
2.2 Related Studies . . . . .	11
2.3 Materials and Methods . . . . .	13
2.3.1 Experimental Setup . . . . .	13
2.3.2 Force Sensor Gravity Biasing . . . . .	16
2.3.3 Non-linear Impedance Matching Approach (NIMA) . . . . .	18
2.4 Results and Discussions . . . . .	20

2.5	Summary	23
<b>3</b>	<b>Neural Network-Based Force Estimation for Realistic Haptic Feedback in Robotic-Assisted Laparoscopy</b>	<b>24</b>
3.1	Objective and Contribution	24
3.2	Related Studies	25
3.3	Methodology	27
3.3.1	Experimental Setup	27
3.3.2	Non-linear Impedance Matching Approach (NIMA)	30
3.3.3	Force Sensor Gravity Biasing	35
3.3.4	Tool-tissue Interacting Force Extraction	37
3.4	Validation Study	45
3.5	Discussions	51
3.6	Summary	53
<b>4</b>	<b>Conclusion and Future Works</b>	<b>54</b>
4.1	Conclusions	54
4.2	Future Works	55
	<b>Bibliography</b>	<b>58</b>
	<b>Appendix A</b>	<b>62</b>
.1	Appendix	63

# List of Figures

Figure 1.1	Minimally invasive surgery versus traditional surgery (All rights reserved by Neoalta Specialty Clinic). . . . .	2
Figure 1.2	DaVinci robotic laparoscopic setup. . . . .	3
Figure 2.1	The proposed NIMA-based force feedback architecture for robot-assisted laparoscopy. The leader module provides surgeons with an interface to interact with, generating the motions to control surgical instruments and receiving haptic feedback simultaneously in real-time. The follower module consists of robotic arms and surgical instruments that deliver the motions and actuate on patients' tissues. . . . .	14
Figure 2.2	(a) The surgical simulation environment with an abdominal dummy, Kinova gen3 robots, surgical tools (i.e. forceps and scissors), instrument adapters, trocars, and pick-and-place surgery training items. (b) The developed surgeon console with adjustable omega.7 haptic devices, an HD display, and an adjustable armrest. . . . .	15
Figure 2.3	Comparison between the norm of rendered (IMA, NIMA) and measured (DFR) forces during contact and contactless interactions between surgical tool-tip and mock tissues. The motion and motionless interactions refer to the human hand holding and releasing the haptic controller. . . . .	21
Figure 2.4	Error distributions for IMA and NIMA methods, with their corresponding fits. . . . .	22
Figure 3.1	System architecture of the presented robot-assisted laparoscopy setup. . . . .	27
Figure 3.2	a) The developed surgeon's console with haptic devices. b) The simulated surgical setup, featuring a mannequin, force sensors, an optical tracker, a laparoscope, surgical tools with instrument adapters, and a tissue surrogate. . . . .	28

Figure 3.3	The proposed NIMA-based force feedback for haptic-enabled surgical robotics.	30
Figure 3.4	Free Body Diagram of the Robotic Laparoscopic Setup During a Typical Task.	33
Figure 3.5	The proposed NIMA-based force feedback for haptic-enabled surgical robotics.	37
Figure 3.6	Graphical representation of the experimental results demonstrating the relationship between the coordinate systems based on force measurements. . . . .	39
Figure 3.7	Experimental setup for determining the relationship between the coordinate systems. This setup showcases the initial configuration of the robotic arm, tissue surrogate, and force sensors. . . . .	40
Figure 3.8	An internal view of the mannequin illustrating the setup for Experiment 2. This setup is designed to acquire data for training a neural network to compute tool-tissue interaction forces. . . . .	42
Figure 3.9	The setup for Experiment 2, showing the arrangement of robotic arms, tissue surrogate, and force sensors for capturing tool-tissue interaction data. . . . .	43
Figure 3.10	Training and validation loss over 1000 epochs, demonstrating convergence and generalization of the neural network model. . . . .	45
Figure 3.11	Illustration of the forces in the Y direction: (a) forces in the Y direction with respect to KBR and (b) comparison of forces in the Y direction. . . . .	47
Figure 3.12	Illustration of the model's performance in the X, Y, and Z directions. . . . .	48
Figure 3.13	Illustration of the trained neural network (NN) model's performance in extracting tip forces along the (a) X, (b) Y, and (c) Z directions, and (d) the residuals, highlighting its accuracy and statistical reliability. . . . .	48
Figure 3.14	Accuracy of the neural network (NN) model in capturing and subtracting frictional forces at the Remote Center of Motion (RCM) in the X direction, enabling precise extraction of tip forces for force rendering. . . . .	49
Figure 3.15	Accuracy of the neural network (NN) model in capturing and subtracting frictional forces at the Remote Center of Motion (RCM) in the Y direction, enabling precise extraction of tip forces for force rendering. . . . .	50

Figure 3.16 Accuracy of the neural network (NN) model in capturing and subtracting frictional forces at the Remote Center of Motion (RCM) in the $Z$ direction, enabling precise extraction of tip forces for force rendering. . . . .	51
Figure 3.17 A histogram illustrating the effectiveness of the neural network (NN) model in accurately capturing forces at the Remote Center of Motion (RCM), facilitating the precise extraction of tool-tissue interaction forces. . . . .	52
Figure 3.18 A comparison between the rendered force using NIMA and the measured force with DFR as the ground truth. . . . .	52
Figure .1 Design of the surgeon console used in the robot-assisted laparoscopic system developed to in this research. . . . .	63
Figure .2 The surgeon console designed, assembled, and used in the robot-assisted laparoscopic system developed in this research. . . . .	64
Figure .3 The Adapter designed, 3D printed in-house, and used in the Follower Module: Integration with 4 Dynamixel Motors as the Main Actuation Unit for Surgical Tool Control. . . . .	65
Figure .4 The laparoscope holder designed, fabricated, and used in the Follower Module: a flange to connect the laparoscope to Kinova robotic arms. . . . .	66

# List of Tables

Table 3.1 Table of related studies with accuracy. . . . . 26

# Chapter 1

## Introduction

### 1.1 Background

#### 1.1.1 Minimally Invasive Surgery (MIS)

Minimally invasive surgery (MIS) has revolutionized the field of surgical interventions, offering significant advantages over traditional open surgical techniques. The fundamental principle of MIS is to reduce the physical trauma associated with surgical procedures, thereby minimizing postoperative pain, shortening recovery times, and improving overall patient outcomes. This evolution in surgical practice began with conventional laparoscopic techniques, which utilize small incisions and specialized instruments to perform surgeries with less disruption to the body's tissues. Over the past few decades, the introduction of robotic-assisted surgical systems has further enhanced the capabilities of minimally invasive procedures, allowing for greater precision and control during complex surgeries [1].

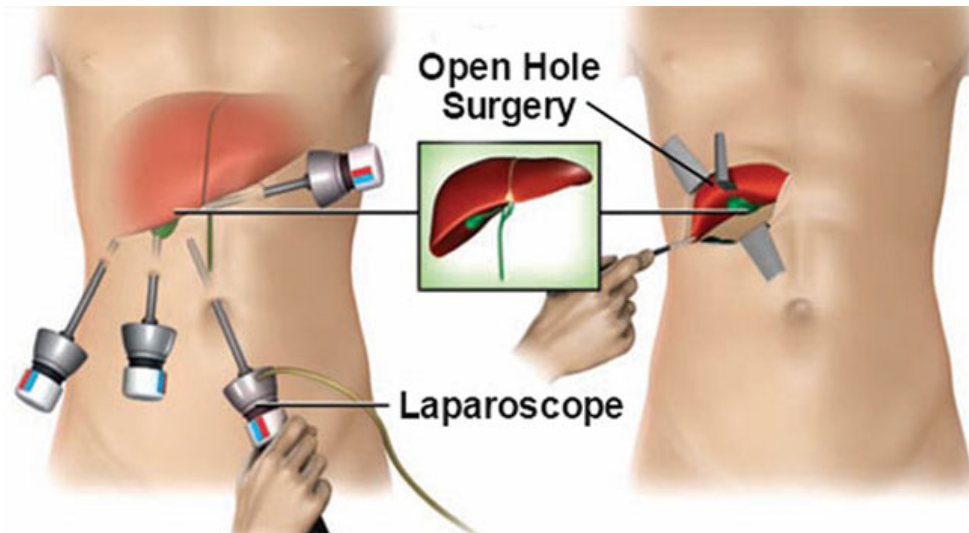


Figure 1.1: Minimally invasive surgery versus traditional surgery (All rights reserved by Neoalta Specialty Clinic).

### 1.1.2 Robot Assisted Laparoscopic surgery

Robotic-assisted laparoscopic surgery, particularly with systems like the da Vinci Surgical System, has gained prominence in various surgical specialties, including gynecology, urology, and general surgery. The robotic platform provides surgeons with a three-dimensional view of the surgical field and allows for enhanced dexterity through wristed instruments, which can articulate in ways that human hands cannot [2]. This technological advancement has made it possible to perform intricate procedures with improved visualization and reduced intraoperative complications. For instance, studies have shown that robotic-assisted techniques can lead to lower blood loss, reduced hospital stays, and quicker recovery times compared to traditional laparoscopic approaches [3].

The application of robotic-assisted laparoscopic procedures has been particularly notable in the treatment of various cancers. For example, in gynecologic oncology, robotic-assisted hysterectomy has been associated with improved surgical outcomes, including reduced postoperative complications and shorter recovery times[4]. Similarly, in urological surgeries, robotic-assisted techniques have demonstrated advantages in procedures such as prostatectomy and nephrectomy, where precision is paramount [5]. The ability to perform complex resections with minimal tissue disruption has

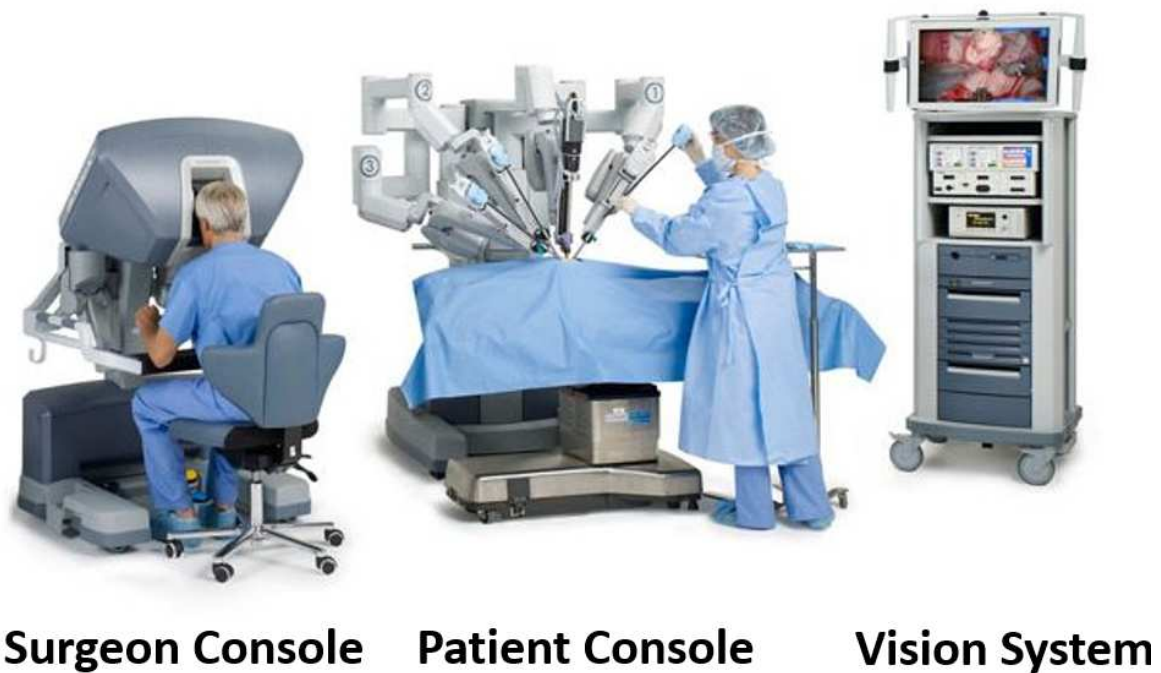


Figure 1.2: DaVinci robotic laparoscopic setup.

made robotic surgery an attractive option for oncological interventions, where preserving surrounding healthy tissue is crucial for patient recovery and long-term outcomes [6].

In addition to oncological applications, robotic-assisted laparoscopic surgery has been successfully employed in various other fields, including colorectal surgery and bariatric procedures. The technique of complete mesocolic excision (CME) for colon cancer, for instance, has been enhanced by robotic assistance, allowing for meticulous dissection and central vascular ligation with reduced morbidity[7]. Moreover, the use of robotic systems in bariatric surgery has shown promising results in weight loss outcomes and postoperative recovery, further solidifying the role of robotic-assisted techniques in diverse surgical disciplines [8].

As the field of robotic surgery continues to evolve, ongoing research is essential to establish clear guidelines regarding its use, particularly in comparison to traditional laparoscopic techniques. Meta-analyses and systematic reviews are increasingly being conducted to evaluate robotic-assisted procedures' safety, efficacy, and cost-effectiveness across various surgical specialties [9]. These studies aim to provide a comprehensive understanding of when robotic assistance is most beneficial and to identify potential areas for improvement in surgical training and technology [6].

In conclusion, minimally invasive surgery, particularly through robotic-assisted techniques, represents a significant advancement in surgical practice. The benefits of reduced trauma, improved precision, and enhanced recovery times make robotic surgery an appealing option for many patients. However, careful consideration of cost, complexity, and the specific surgical context is necessary to ensure that the adoption of robotic systems is justified and beneficial. As the body of evidence continues to grow, the surgical community must engage in ongoing dialogue regarding the optimal use of robotic-assisted laparoscopic procedures to maximize patient outcomes and healthcare efficiency.

### **1.1.3 Clinical Need for Force Feedback in Robot-assisted Laparoscopic Surgery**

The clinical need for force feedback in robotic surgery is increasingly recognized as a critical factor in enhancing surgical precision and safety. Haptic feedback is essential for the surgeon's ability to gauge the force applied to tissues during surgical manipulation using robotic surgical systems, such as the da Vinci Surgical System. Lack of tactile sensation can lead to increased risks of tissue damage and complications, highlighting an unmet need in the field of robotic surgery [10].

Force feedback is crucial for several reasons. Firstly, it allows surgeons to differentiate between various tissue types and to assess the mechanical properties of tissues, such as stiffness and elasticity, which are vital for safe and effective surgical interventions [11]. The absence of this feedback can result in excessive force application, potentially causing unintended trauma to delicate structures and leading to postoperative complications [12]. For instance, studies have shown that surgeons often apply more force than necessary when operating without haptic feedback, which can increase the risk of injury to surrounding tissues [13]. Furthermore, the reliance on visual feedback alone is insufficient, as it does not provide the nuanced information that tactile feedback offers, particularly in complex surgical scenarios [14].

The integration of force feedback into robotic surgical systems presents a promising avenue for enhancing surgical precision and safety. However, the addition of force rendering capabilities can lead to instability in the system, which poses significant challenges in meeting regulatory standards for surgical devices. This instability arises from several factors, including the complexity of accurately sensing and rendering forces, the potential for feedback loops that can distort the surgeon's control, and the inherent variability in tissue response during surgical manipulation.

One of the primary concerns with implementing force feedback in robotic surgery is the risk of introducing instability into the control system. Research has indicated that when force feedback is not carefully calibrated, it can lead to distorted motion control, where the surgeon's commands are compromised by the feedback forces being rendered [15]. For instance, Farkhatdinov and Ryu demonstrated that feedback based on obstacle range information could prevent accurate motion control of mobile robots, suggesting that similar issues could arise in surgical contexts where precise manipulation is critical [15]. This distortion can result in unintended movements or excessive force application, increasing the risk of tissue damage and complications during surgery [16].

Moreover, the regulatory hurdles for surgical devices are stringent, requiring extensive validation of safety and efficacy before approval. The introduction of force feedback systems must demonstrate not only that they enhance surgical performance but also that they do not compromise patient safety. The potential for feedback-induced instability complicates this validation process. For example, the lack of tactile feedback in current robotic systems has been associated with prolonged operative times and increased difficulty in performing force-sensitive tasks, which could lead to adverse clinical outcomes [17]. Regulatory bodies may view the introduction of force rendering as a risk factor, particularly if it is associated with increased variability in surgical performance or complications.

Additionally, the technical challenges of developing reliable force feedback systems further contribute to the unmet regulatory needs. Accurate force sensing and rendering require sophisticated sensor technologies that can effectively measure the forces applied during surgery and provide real-time feedback to the surgeon [18]. However, the integration of such technologies into existing robotic systems is fraught with difficulties, including ensuring that the feedback is intuitive and does not overwhelm the surgeon during critical moments of surgery [14]. The complexity of these systems can lead to unpredictable behaviors, which regulatory agencies are likely to scrutinize closely.

Furthermore, the clinical implications of force feedback systems must be thoroughly evaluated. While the potential benefits of enhanced tactile feedback are clear, the risks associated with instability must be addressed. For instance, Abiri et al. highlighted that the loss of haptic feedback, combined with the ability of robotic systems to apply strong forces, can lead to increased risks of

tissue damage and mistakes during surgery [16]. Such outcomes could raise red flags during the regulatory review process, as they directly impact patient safety and surgical efficacy.

In conclusion, while the addition of force rendering to robotic surgical systems holds significant potential for improving surgical outcomes, it also introduces challenges related to system stability and regulatory compliance. The risks associated with feedback-induced instability, coupled with the technical complexities of implementing reliable force feedback, create significant hurdles that must be overcome before these systems can be widely adopted in clinical practice. Ongoing research and development efforts are essential to address these issues, ensuring that any advancements in force feedback technology enhance rather than compromise surgical safety.

## **1.2 Research Objectives**

The primary objective of this research is to develop and validate a robust haptic feedback system for robotic-assisted laparoscopic surgery (RALS) that addresses the clinical need for force feedback while mitigating risks associated with system instability and regulatory non-compliance. Specifically, this study aims to:

- (1) To design and implement a robust experimental setup, including custom surgical tools, Kinova robotic arms, Omega.7 haptic controllers, and Bota force sensors, to simulate realistic surgical environments and validate the effectiveness of NIMA.
- (2) To develop a safe and reliable haptic feedback method for robotic-assisted laparoscopic surgery.
- (3) To propose and validate a neural network-based tool-tissue force estimation method, enabling precise extraction of interaction forces by compensating for extraneous forces, such as friction at the Remote Center of Motion (RCM) and gravitational effects.
- (4) To achieve an improvement in force rendering accuracy compared to the other methods, and to validate that through extensive experiments.
- (5) To enhance the realism and stability of haptic feedback systems for robotic surgery, providing a transformative solution for overcoming the absence of tactile sensation in existing commercial robotic systems.

- (6) To achieve seamless coordination between the movements of the controller and the laparoscope's view, ensuring intuitive and precise control during teleoperated surgical tasks.

This research seeks to bridge the gap between the potential benefits of haptic feedback in robotic surgery and the technical, clinical, and regulatory challenges that currently limit its widespread adoption. By doing so, it aims to advance the field of minimally invasive surgery and improve patient outcomes across various surgical disciplines.

### **1.3 Publications**

The following list summarizes the author's contributions during this research:

#### **Journal paper**

- Neural Network-Based Force Estimation for Realistic Haptic Feedback in Robotic-Assisted Laparoscopy (Will be submitted to "IEEE Transactions on Automation Science and Engineering" by Jan,30th 2025)

#### **Conference papers**

- Mazidi, A., Ramos, A.C., Sayadi, A., Dargahi, J., Barralet, J., Feldman, L.S. and Hooshlar, A., 2024, September. Nonlinear Impedance Matching Approach (NIMA) for Robust Haptic Rendering During Robotic Laparoscopy Surgery. In 2024 10th IEEE RAS/EMBS International Conference for Biomedical Robotics and Biomechatronics (BioRob) (pp. 1809-1814). IEEE.
- Mazidi, A., Ramos, A.C., Sayadi, A., Dargahi, J., Barralet, J., Feldman, L.S. and Hooshlar, A."Nonlinear Impedance Matching Approach (NIMA) for Robust Haptic Rendering During Robotic Laparoscopy Surgery." 2023 IEEE/RSJ International Conference on Intelligent Robots and Systems (IROS), Detroit, Michigan, USA .
- Mazidi, A., Ramos, A.C., Sayadi, A., Dargahi, J., Barralet, J., Feldman, L.S. and Hooshlar, A. "Nonlinear Impedance Matching Approach (NIMA) for Robust Haptic Rendering During Robotic Laparoscopy Surgery." 2024, Presented at The Hamlyn symposium, London, UK.

## 1.4 Thesis layout

This thesis is prepared in manuscript-based style according to the "Thesis Preparation and Thesis Examination Regulations (version-2022) for Manuscript-based Thesis" of the School of Graduate Studies of Concordia University. This dissertation includes two chapters with the following contents:

**Chapter 2** presents the development and validation of the Nonlinear Impedance Matching Approach (NIMA) for robust haptic rendering in robotic-assisted laparoscopic surgery. This chapter introduces a novel nonlinear framework to enhance force rendering fidelity, addresses the limitations of linear impedance models, and validates NIMA through extensive experiments. The chapter's major contributions include:

- Developing a nonlinear framework for precise haptic feedback during robot-assisted laparoscopic surgery, demonstrating an 85% improvement in force rendering accuracy compared to linear methods.
- Designing and implementing a state-of-the-art experimental setup featuring Kinova robotic arms, Omega.7 haptic controllers, and custom surgical tools to validate NIMA under realistic surgical scenarios.

This chapter is based on the following publication:

- (1) Mazidi, Aiden, et al. "Nonlinear Impedance Matching Approach (NIMA) for Robust Haptic Rendering During Robotic Laparoscopy Surgery." 2024 10th IEEE RAS/EMBS International Conference for Biomedical Robotics and Biomechatronics (BioRob). IEEE, 2024. [19]

**Chapter 3** focuses on identifying and quantifying all forces acting on surgical tools during robotic-assisted laparoscopic surgery. It addresses challenges such as frictional forces at the RCM and gravitational biases by proposing a neural network-based tool-tissue force estimation method. This chapter also validates NIMA as a safe and effective nonlinear force-rendering method. The key contributions of this chapter are:

- Designing and implementing a comprehensive experimental setup to simulate realistic surgical conditions for tool-tissue force estimation.

- Training a neural network to isolate precise interaction forces, achieving a Mean Absolute Error (MAE) of 0.1 N in estimating tool-tissue interaction forces.
- Demonstrating a 95% improvement in force rendering fidelity and eliminating haptic kick-back using NIMA, thereby improving safety and stability in robotic-assisted surgical systems.

This chapter includes results from the following key experiments:

- (1) Establishing a unified coordinate system for forces through calibration methods validated using tool-tissue interaction forces.
- (2) Training and validating a neural network model for extracting tool-tissue forces, with accuracy verified through experiments and statistical analyses.

The contents of this thesis provide a cohesive narrative addressing significant gaps in the integration of haptic feedback into robotic-assisted laparoscopic systems. **Chapter 2** introduces the innovative NIMA method, while **Chapter 3** extends its application by isolating and quantifying precise tool-tissue forces, thus paving the way for its adoption in commercial robotic surgical platforms.

## **Chapter 2**

# **Nonlinear Impedance Matching**

# **Approach (NIMA) for Robust Haptic**

# **Rendering during Robotic Laparoscopy**

# **Surgery**

## **2.1 Objective and Contributions**

The primary objective of this chapter is to develop and validate the Nonlinear Impedance Matching Approach (NIMA) for robust and accurate haptic feedback during robotic-assisted laparoscopic surgery. Specifically, this chapter aims to address the following thesis objectives:

- To develop a safe and reliable haptic feedback method for robotic-assisted laparoscopic surgery by introducing a nonlinear framework that improves force rendering fidelity.
- To propose and validate a neural network-based tool-tissue force estimation method, enabling precise extraction of interaction forces by compensating for extraneous forces, such as friction at the Remote Center of Motion (RCM) and gravitational effects.
- To achieve an improvement in force rendering accuracy compared to existing methods and

validate this enhancement through extensive experiments.

The contributions of this chapter are as follows:

- (1) Developed the Nonlinear Impedance Matching Approach (NIMA), a novel method for force rendering in robotic-assisted laparoscopic surgery, effectively addressing the limitations of linear impedance models by incorporating nonlinear dynamics to enhance accuracy and stability.
- (2) Designed and implemented an experimental framework, including state-of-the-art components such as Kinova robotic arms, Omega.7 haptic controllers, and custom-adapted surgical tools, to evaluate the performance of NIMA in realistic surgical scenarios.
- (3) Demonstrated a significant improvement in force rendering accuracy, achieving a Mean Absolute Error (MAE) of 0.03 N, representing an 85% enhancement compared to the previously developed Linear Impedance Matching Approach (IMA).
- (4) Validated the elimination of undesirable phenomena such as haptic kickback, enhancing user safety and comfort during haptic interactions.
- (5) Established a robust framework for integrating NIMA-based haptic feedback into robotic-assisted laparoscopic systems, paving the way for advancements in both surgical training and clinical applications.

## 2.2 Related Studies

There is a recognized need for advancements in haptic technology for robot-mediated surgery to enhance patient care and improve robotic surgical procedures [20]. Incorporating haptic feedback in teleoperated robot-assisted surgical systems presents promising clinical and scientific opportunities, including active operator assistance and automatic tissue property acquisition [21]. However, the absence of haptic feedback in current teleoperated surgical robots due to the potential destabilization of the closed-loop controller has limited its expected clinical benefits [22]. The value of haptic

feedback in robotics is widely acknowledged [23], but the necessity of haptics in surgical procedures is still questioned [24].

Incorporating haptic feedback in robotic surgery has been shown to enhance the consistency, precision, and performance of surgical tasks such as knot tying, reducing the risk of tissue damage [16]. Additionally, haptic feedback has been demonstrated to improve surgical outcomes by enabling better dexterous motion and enhancing visual feedback, ultimately improving precision and reducing risk for patients [23, 25, 26].

The regulatory validation of haptic systems as a "human-in-the-loop" component presents significant challenges, including the complexity of validating inter-subject dynamics variations. This complexity arises from the design of the system, which incorporates human interaction, making it difficult to standardize and validate [21]. Additionally, the variability due to human subjects and grip-force variation further complicates the regulatory validation process, as these factors introduce uncertainties that need to be accounted for in the validation of haptic systems [27]. These challenges have impeded the commercialization of haptic systems, particularly in the context of surgical robotics, where stringent regulatory requirements must be met to ensure patient safety and system effectiveness.

The impedance-matching approach (IMA) for force feedback estimation and rendering does not incorporate the "human" as a component, as it focuses on providing force feedback using sensory substitution techniques, avoiding the use of actuators for force feedback on the leader side [28]. This approach achieves indirect force control via closed-loop position control without explicit closure of a force feedback loop, which distinguishes it from other control schemes that offer the possibility of controlling the contact force to a desired value through the closure of a force feedback loop [29].

An impedance-matching model-in-the-loop simulation has been described in previous publications, outlining its concept, salient features, and sample applications [30]. Additionally, a proposed approach combines object recognition from a tactile appearance with a purposeful haptic exploration of unknown objects to extract appearance information, demonstrating a different perspective on haptic feedback [31]. Furthermore, haptic rendering algorithms play a crucial role in eliminating oscillations of feedback force and rendering high-fidelity feedback force to users, contributing to the evaluation of haptic feedback accuracy in robotic teleoperation [32].

We have previously shown the accuracy and stability of the linear IMA method for a single force component in [33]. In this work, we propose a general non-linear IMA (NIMA) framework, as shown in Fig. 3.3, that accounts for the impedance parameters when the instrument-tissue interaction is not linear. In addition, in this study, we detail the significant achievements of our research, specifically focusing on the implementation and validation of the novel NIMA method. Our comprehensive testing phase has yielded positive results, affirming the method’s accuracy in precisely controlling 3D contact forces and executing motion commands. This level of precision was achieved in the context of a commercially available robot-assisted laparoscopic system, underscoring the practical applicability and potential of the NIMA method in enhancing surgical performance and outcomes. Through evaluations, we demonstrate the NIMA method’s capability to improve the precision and reliability of robotic-assisted surgical procedures, paving the way for its broader adoption in the medical field.

## **2.3 Materials and Methods**

### **2.3.1 Experimental Setup**

The experimental equipment was meticulously crafted to replicate a surgical setting by incorporating state-of-the-art components. Two Kinova Gen3 (7 DOF) robotic arms Kinova robots, renowned for their advanced manipulation capabilities, played a critical role in executing precise and controlled movements of surgical tools. As shown in Fig. 3.2(a), these robots emulate human hand dexterity thanks to their 6 degrees-of-freedom and ample workspace, which is critical in surgical experiments as the motions replicated by the robots mimic those of the human hand with high accuracy. Three 6-axis force-torque sensors (SensONE, Bota Systems) were placed at the end-effectors for force measurement. In addition, dedicated carts were designed and built to provide a base, stability, and maneuverability for the robotic arms, ensuring optimal positioning throughout experimental procedures. DaVinci SI surgical tools (Intuitive) were adapted to robotic arms for tailored surgical tasks. The tools were integrated into the robotic arms using custom-designed adapters to ensure a seamless functionality that meets clinical standards. Classic tooltips such as forceps were adapted to provide the needed dexterity and usability. The tools were powered

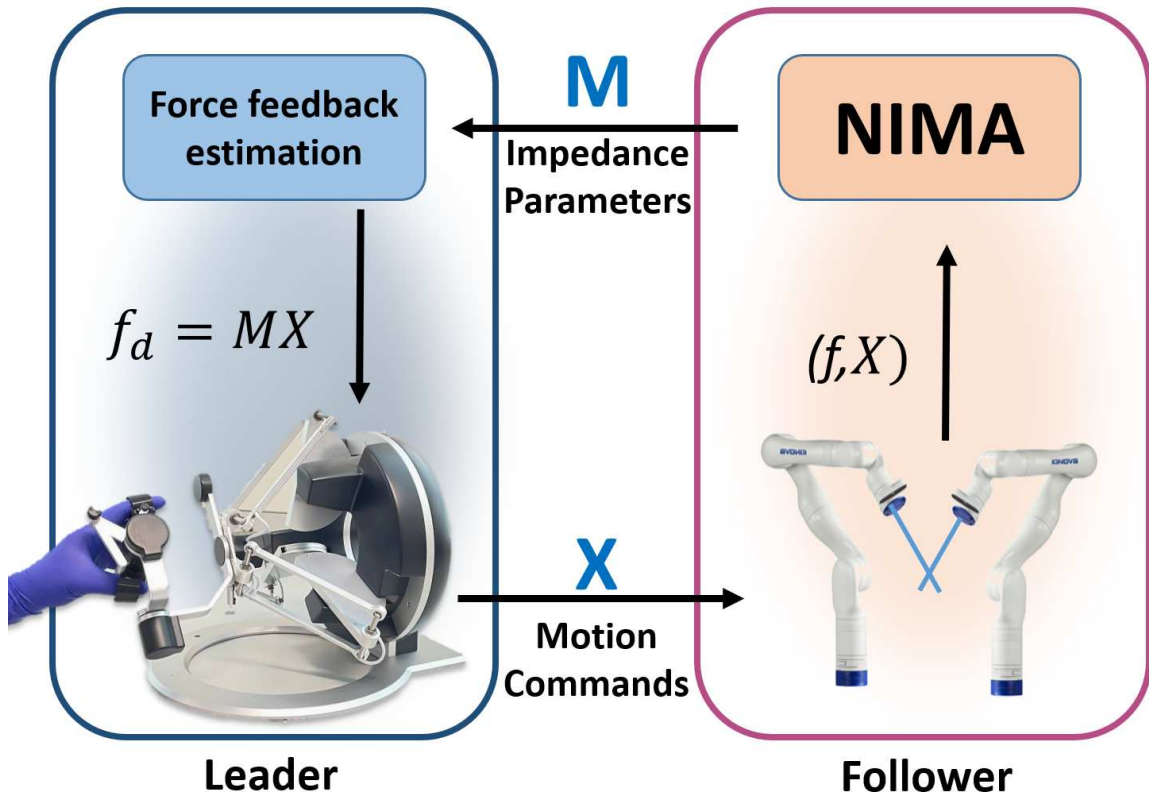


Figure 2.1: The proposed NIMA-based force feedback architecture for robot-assisted laparoscopy. The leader module provides surgeons with an interface to interact with, generating the motions to control surgical instruments and receiving haptic feedback simultaneously in real-time. The follower module consists of robotic arms and surgical instruments that deliver the motions and actuate on patients' tissues.

by four Dynamixel actuators (ROBOTIS) on each robotic arm, enabling nuanced control during trials. These actuators are responsible for controlling the tip of the surgical tools to enable precise grasping.

Two Omega.7 haptic controllers (Force Dimension) served as the interface between the human operator and the robotic arms, by translating hand motions into precise surgical movements. These haptic devices provide high-resolution position encoding with sub-millimetre accuracy. An adjustable surgeon console was also designed and built to provide ergonomic access to the controllers.

To ensure anatomical fidelity, a translucent bespoke mannequin was strategically integrated with tissue-representative objects, as shown in Fig. 3.2, simulating structural complexities encountered in actual surgical scenarios, such as pick-and-place and suturing tasks, to create challenging experimental conditions similar to those in real surgical procedures.



For quantifying and analyzing forces during simulated tasks, Boto force sensors were placed at the tip of each robotic arm. These sensors captured essential force data, offering insights into mechanical interactions between the surgical tool and the tissue-representative objects.

The in-house designed adaptable surgical console, as shown in Fig. 3.2 served as the central control hub, facilitating seamless communication and coordination among all components. This console enabled the integration and synchronization of the controllers, robotic arms, surgical tools, Dynamixel actuators, and force sensors, ensuring a cohesive and efficient experimental setup.

### 2.3.2 Force Sensor Gravity Biasing

For integrating force feedback into robotic laparoscopic surgery, force sensor system identification is crucial for sensor biasing and mass compensation. These two factors ensure precise and accurate measurement of the reflecting forces between the instruments and the tissue. The system identification process integrated in this study utilizes IMU data to estimate the spatial orientation of the end effector. This allows for the effective implementation of gravitational biasing techniques, which eliminate the effects of gravity on the robotic instruments. By leveraging the IMU data, the system can accurately determine the orientation of the end effector (roll, pitch, and yaw), which is critical for biasing the gravitational forces acting on the robotic instruments. For the sake of simplicity, the proposed method only uses the accelerations in three directions to find the Roll and Pitch angles in the end effector orientation, without relying on temporal integration of angular velocities [34]. The angles mentioned above were extracted in real time using these equations:

$$\alpha = \text{atan2}(a_y, a_z) \quad (1)$$

$$\beta = \text{atan2}\left(-a_x, \sqrt{a_y^2 + a_z^2}\right) \quad (2)$$

where  $\alpha$  is the angle of rotation around the x-axis of the world's coordinate system,  $\beta$  is the angle of rotation around the y-axis, and  $a_x$ ,  $a_y$ , and  $a_z$  represent the acceleration values in the  $x$ ,  $y$ , and  $z$  directions, respectively. For gravitational compensation and sensor biasing, a series of maneuvers were designed to cover every possible configuration of the robot's end effector during

a surgical task. These maneuvers were performed with all the relevant equipment, including the surgical tool, four Dynamixel actuators, and the custom-designed adapter, installed on each robot. Throughout the task, force readings from the sensor and the angles of the end effector were captured and recorded. This data was then used for extracting a model for calculating the gravitational forces and sensor bias in any orientation of the surgical tool. The model extraction process is critical as it forms the basis for implementing the biasing techniques to counteract the effects of gravity on the robotic instruments. The formulation for the extracted model is in the form of:

$$\mathbf{AC} = \mathbf{B} \quad (3)$$

where  $\mathbf{A}$  represents the system's configuration,  $\mathbf{C}$  is the matrix of unknown coefficients, and  $\mathbf{B}$  is the sensor readings. Then:

$$\mathbf{A} = \begin{pmatrix} \sin \alpha_{t_1} & \cos \alpha_{t_1} & \sin \beta_{t_1} & \cos \beta_{t_1} & 1 \\ \sin \alpha_{t_2} & \cos \alpha_{t_2} & \sin \beta_{t_2} & \cos \beta_{t_2} & 1 \\ \vdots & \vdots & \vdots & \vdots & \vdots \\ \sin \alpha_{t_n} & \cos \alpha_{t_n} & \sin \beta_{t_n} & \cos \beta_{t_n} & 1 \end{pmatrix}_{n \times 5} \quad (4)$$

$$\mathbf{C} = \begin{pmatrix} C_{1x} & C_{1y} & C_{1z} \\ C_{2x} & C_{2y} & C_{2z} \\ C_{3x} & C_{3y} & C_{3z} \\ C_{4x} & C_{4y} & C_{4z} \\ C_{5x} & C_{5y} & C_{5z} \end{pmatrix}_{5 \times 3} \quad (5)$$

$$\mathbf{B} = \begin{pmatrix} F_{X_{t_1}} & F_{Y_{t_1}} & F_{Z_{t_1}} \\ F_{X_{t_2}} & F_{Y_{t_2}} & F_{Z_{t_2}} \\ \vdots & \vdots & \vdots \\ F_{X_{t_n}} & F_{Y_{t_n}} & F_{Z_{t_n}} \end{pmatrix}_{n \times 3} \quad (6)$$

where  $F$  represents the sum of the gravitational force and sensor bias collected from the force sensor during the robot's maneuver for a given position.

To obtain the matrix of coefficients  $\mathbf{C}$ , which is crucial for our model, we can solve equation 3 using the pseudo-inverse of  $\mathbf{A}$  as follows:

$$\mathbf{C} = \mathbf{A}^\dagger \mathbf{B} \quad (7)$$

where  $\mathbf{A}^\dagger = \mathbf{A}^T (\mathbf{A}\mathbf{A}^T)^{-1}$  is the pseudo-inverse of  $\mathbf{A}$ .

Once we have obtained the matrix of coefficients, we can implement the gravitational biasing techniques based on the model extracted from the IMU data.

The successful integration of these techniques will enable the robotic instruments to bias for the gravitational forces, ensuring more precise and accurate movements during laparoscopic surgery.

### 2.3.3 Non-linear Impedance Matching Approach (NIMA)

This study introduces a nonlinear impedance matching approach (NIMA) for providing force feedback in remote surgical robotics as an alternative to direct force reflection (DFR). The concept of NIMA is based on the real-time identification of nonlinear tool-tissue contact impedance parameters  $\mathbf{M}$  at the follower module and relays those to the leader module. Meanwhile, motion commands  $\mathbf{X}$  are relayed to the follower module where a representative laparoscopic instrument interacts with a mannequin as a representative soft tissue model. Without loss of generality and for the sake of simplicity, we incorporated a polynomial nonlinear impedance model to identify the NIMA parameters  $\mathbf{M}$ . The contact force  $\mathbf{f} \in \mathbb{R}^{3 \times 1}$  was modelled as the response of a nonlinear impedance hyper-surface to a given motion command  $\mathbf{X}$  according to the following equation:

$$\mathbf{f} = \mathbf{M}\mathbf{X} = \mathbf{M} \begin{pmatrix} \mathbf{x}_N^* & \mathbf{y}_N^* & \mathbf{z}_N^* \end{pmatrix}_{1 \times 9N}^T \quad (8)$$

where  $^T$  is the transpose operator,  $x$ ,  $y$ , and  $z$  are the motion commands (i.e., incremental position changes of the instrument during a time window  $\delta t$ ),  $^*_N$  is the augmented state operator of degree  $N$  defined as:

$$\mathbf{u}_N^* = \begin{pmatrix} u & \dot{u} & \ddot{u} & \cdots & u^N & \dot{u}^N & \ddot{u}^N \end{pmatrix}_{3N \times 1} \quad (9)$$

and  $\mathbf{M}$  is the NIMA impedance parameters of the form:

$$\mathbf{M} = \begin{pmatrix} \mathbf{m}_x & \mathbf{0} & \mathbf{0} \\ \mathbf{0} & \mathbf{m}_y & \mathbf{0} \\ \mathbf{0} & \mathbf{0} & \mathbf{m}_z \end{pmatrix}_{3 \times 9N} \quad (10)$$

where  $\mathbf{m}_i \in \mathbb{R}^{1 \times 3N}$  as the vector of NIMA impedance parameters and  $\mathbf{0} \in \mathbb{R}^{1 \times 3N}$  as the zero vector.

It is worth assuming there is no cross-talk between orthogonal components of the tool-tissue forces in the  $x$ -,  $y$ -,  $z$ - directions. Nevertheless, this can be achieved by adding non-zero parameters of the form  $\mathbf{m}_i$  for modelling the cross-talk. To identify the unknown  $\mathbf{M}$  in real-time, a rolling time window of  $\delta t = 300$  ms was considered. Evidence suggests that a delay of less than 300 ms might not be perceivable for surgeons in leader-follower architectures [35]. Thus, a 300ms time window could simulate a worst-case scenario for updating the impedance parameters (and forces). The NIMA parameters  $\mathbf{M}$  were being identified on the fly, over the collected window (i.e. first-in-first-out) of  $n$  sample forces  $\hat{\mathbf{F}} \in \mathbb{R}^{3 \times n}$  and the corresponding motion commands  $\hat{\mathbf{X}}$  using:

$$\mathbf{M} = \hat{\mathbf{F}} \hat{\mathbf{X}}^+ \quad (11)$$

$$\hat{\mathbf{F}} = \begin{pmatrix} \mathbf{f}_{t_0} & \cdots & \mathbf{f}_{t_0 + \delta t} \end{pmatrix}_{3 \times n} \quad (12)$$

$$\hat{\mathbf{X}} = \begin{pmatrix} \mathbf{x}_{t_0} & \cdots & \mathbf{x}_{t_0 + \delta t} \end{pmatrix}_{9N \times n} \quad (13)$$

where  $\hat{\mathbf{X}}^+ = \hat{\mathbf{X}}^T (\hat{\mathbf{X}} \hat{\mathbf{X}}^T)^{-1}$  is the pseudo-inverse of  $\hat{\mathbf{X}}$ .

In this study, the peg transfer task, critical to the Fundamentals of Laparoscopic Surgery (FLS) program [36], was selected for analysis. Throughout this task, two surgical tools were affixed to two robotic arms, while a camera suitable for laparoscopy procedures was mounted on the third arm. The task comprised three distinct phases: Motion with no contact, motion and contact, and

contact with no motion phase. During all phases, the surgical tools remained within the mannequin. However, in the motion with no contact phase, position commands were transmitted from the leader, but there was no physical contact between the surgical tool and the peg. In the subsequent phase, the experiment proceeded by fully grasping the peg and transferring it to the designated bar. In the final phase, contact between the surgical tool and the tissue representative was maintained, while no position commands were sent, meaning that the controller was not being held. This task’s execution entailed capturing the positions, orientations, and velocities of robotic arms using the controllers, with synchronization to the operator’s motion commands achieved at a refresh rate of 1 kHz and a programmatic delay of 300 ms. Force signals were recorded through force sensors (SensOne, Bota Systems) at a sampling rate of 2 kHz. This data facilitated the identification of parameters for the Nonlinear Impedance Matching Approach (NIMA), which were subsequently applied in Eq. 14 to compute and apply the desired three-dimensional force,  $\mathbf{f}_d$  on the haptic device. To optimize the degree of polynomial approximation,  $N$ , for NIMA, five parallel threads with  $N = 1 \cdots 5$  were executed. The selection of  $N$  for each time window was determined based on achieving the minimum norm of the 3D force reconstruction error, ensuring accurate force feedback emulation and improving the surgical simulation experience.

## 2.4 Results and Discussions

The effectiveness of our Nonlinear Impedance Matching Approach (NIMA) in the accurate rendering of forces on haptic devices is demonstrated in Fig. 2.3.

This figure presents a comparison between the forces rendered by the haptic device and the actual forces measured by force sensors. Implementing NIMA resulted in a Mean Absolute Error (MAE) of 0.03 N, showcasing a high fidelity in force feedback, with the errors exhibiting a normal distribution characterized by a Standard Deviation (SD) of 0.08 N. This performance significantly surpasses that of our previous Linear Impedance Matching (IMA) strategy, which recorded an MAE of 0.2 N and an SD of 0.4 N.

A comparative assessment of NIMA against the IMA framework reveals a remarkable 85% improvement in accuracy with the use of NIMA. This enhancement not only highlights the superior

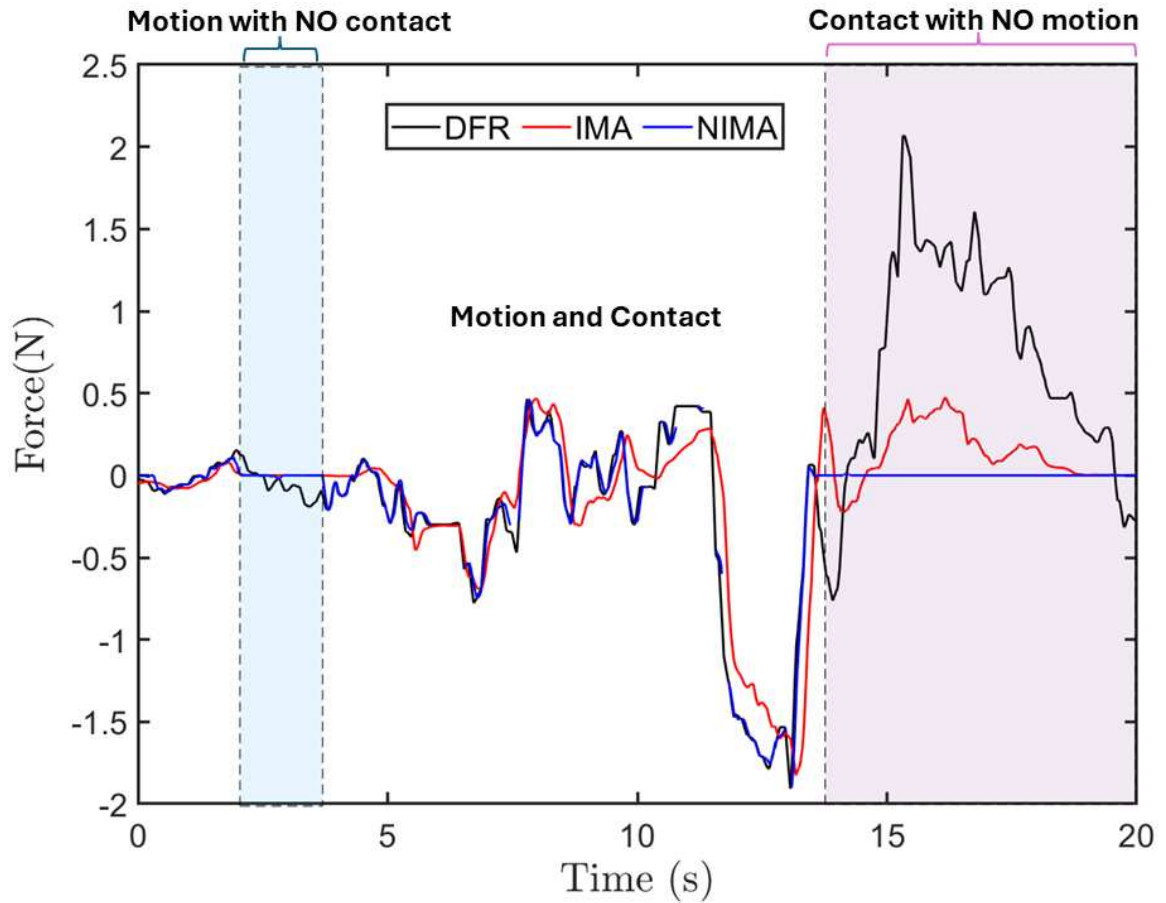


Figure 2.3: Comparison between the norm of rendered (IMA, NIMA) and measured (DFR) forces during contact and contactless interactions between surgical tool-tip and mock tissues. The motion and motionless interactions refer to the human hand holding and releasing the haptic controller.

precision of the nonlinear approach in generating force feedback but also establishes a new standard in the immersion of haptic interactions. The substantial reduction in MAE emphasizes the effectiveness of integrating nonlinear dynamics into impedance-matching processes, thereby advancing the quality and reliability of haptic feedback.

Fig. 2.4 compares the distribution of error between IMA and NIMA and their normal distribution fit.

Moreover, a detailed analysis of the algorithm’s performance throughout the experiment revealed a noteworthy preference for non-linear models, with a non-linear fit being selected in over 64% of the evaluated time windows. This significant reliance on non-linear approaches underscores

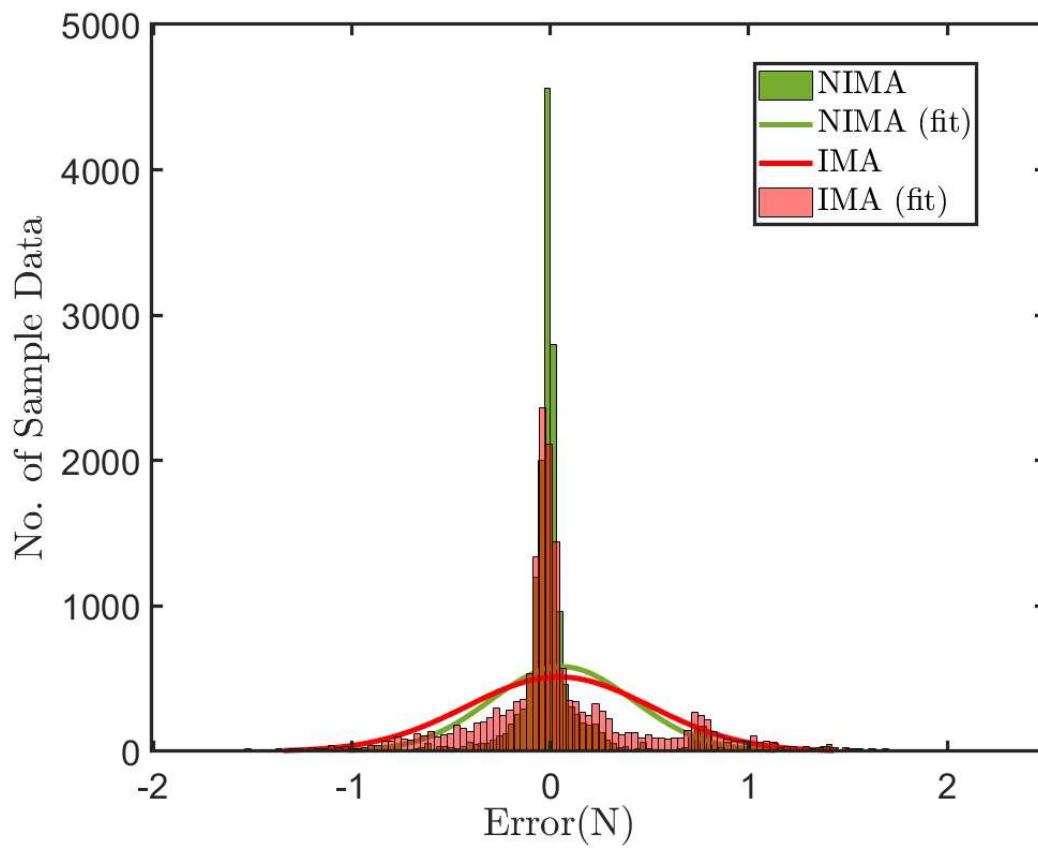


Figure 2.4: Error distributions for IMA and NIMA methods, with their corresponding fits.

the potential inadequacies of the Linear Impedance Matching (IMA) model in capturing the nuanced, dynamic interactions between the surgical tool and tissue. The complexity and variability of these interactions surpass the representational capabilities of linear models, highlighting the intricate nature of tool-tissue forces encountered during laparoscopic procedures. Our findings suggest that the temporal variations of these forces, which are critical for displaying meaningful haptic feedback, are better represented through non-linear modelling, providing an accurate and valuable simulation that resembles actual surgical scenarios.

Throughout our experiments, the phenomenon commonly referred to as "haptic kick" — a sudden, unwelcome jerk felt by the operator upon the release of the haptic device — was notably absent. This observation is consistent with the mechanisms we have previously described [33], wherein the rapid convergence of the system's output force vector,  $\mathbf{X}$ , to zero within a brief time window,  $\delta t$ , upon the user releasing the haptic device ensures that the desired force,  $\mathbf{f}_d$ , also approaches zero. This behaviour effectively neutralizes the potential for a haptic kickback, thereby enhancing the safety and comfort of the operator's experience. The elimination of the haptic kick in our system not only improves user interaction with the haptic device but also represents a significant step forward in developing more sophisticated and user-friendly haptic feedback systems for surgical training simulators.

## 2.5 Summary

The proposed NIMA method is an intrinsically safe force-rendering method for haptics-enabled teleoperation. In this study, most of the major components of a teleoperated system were presented through commercially available robotic teleoperation components.

NIMA will also be used in more channels to include torque feedback. In addition, this work could use the proposed NIMA model in a physics-informed neural network (PINN) model for self-supervised model-free force rendering.

## **Chapter 3**

# **Neural Network-Based Force Estimation for Realistic Haptic Feedback in Robotic-Assisted Laparoscopy**

### **3.1 Objective and Contribution**

The primary objective of this chapter is to identify and quantify all forces acting on the surgical tool during robot-assisted laparoscopic surgery. This involves defining a method to calculate these forces using force sensors placed outside the patient's body while addressing the associated challenges. Additionally, this chapter aims to conduct comprehensive validation studies on the proposed Nonlinear Impedance Matching Approach (NIMA) for force rendering in robot-assisted laparoscopic surgeries.

The key objectives of this chapter are as follows:

- (1) To design and implement a robust experimental setup that integrates custom surgical tools, Kinova robotic arms, Omega.7 haptic controllers, and Bota force sensors. This setup simulates realistic surgical environments to evaluate and validate the Nonlinear Impedance Matching Approach (NIMA).

- (2) To propose and validate NIMA as a safe and effective force-rendering method that incorporates nonlinear dynamics for enhanced haptic feedback.
- (3) To develop a neural network-based tool-tissue force estimation method capable of isolating precise interaction forces by compensating for extraneous forces such as friction at the Remote Center of Motion (RCM) and gravitational effects.
- (4) To demonstrate the superiority of NIMA in improving the realism and stability of haptic feedback compared to traditional linear methods, providing a transformative solution for addressing the absence of tactile sensation in robotic-assisted surgical systems.

This chapter makes significant contributions to the field of haptic feedback and robotic-assisted laparoscopic surgery through the following advancements:

- (1) Developed the Nonlinear Impedance Matching Approach (NIMA) to incorporate nonlinear dynamics, achieving a 95% improvement in force rendering fidelity compared to linear impedance methods and successfully eliminating haptic kickback, thereby enhancing the precision, safety, and stability of haptic feedback in robot-assisted laparoscopic surgeries.
- (2) Proposed and validated a neural network-based tool-tissue force estimation method that isolates precise interaction forces by compensating for extraneous influences such as friction at the Remote Center of Motion (RCM) and gravitational effects, achieving a Mean Absolute Error (MAE) of 0.1 N.
- (3) Demonstrated that NIMA effectively addresses the absence of tactile feedback in commercial robotic surgical systems, improving the realism, responsiveness, and accuracy of force feedback while enabling seamless coordination between surgeon input and the laparoscope's view, paving the way for broader integration into commercial platforms.

These contributions collectively represent a significant step forward in improving the precision, usability, and safety of robotic-assisted surgical systems.

## **3.2 Related Studies**

Table 3.1: Table of related studies with accuracy.

Application	Method	Advantages	Limitations	Accuracy
Laparoscopic Surgery	Vibrotactile and skin-indentation displays [37]	Enhanced tactile perception	Limited experimental validation	Not Reported
Keyhole Endoscopy	Force-sensing at the instrument tip [38]	Improved precision and safety	Integration challenges in complex setups	~90%
Robot-Assisted Surgery	Haptic feedback for teleoperation [39]	Improved surgeon accuracy and reduced fatigue	High cost and system complexity	Not Reported
Neurosurgery	NeuroArm system with haptic corridors [20]	Real-time tactile cues for tissue manipulation	Limited to specific surgical scenarios	Not Reported
Needle Insertion	Force feedback amplification [38]	Enhanced needle control during procedures	Limited clinical testing	~92%
Orthopedic Surgery	MAKO Tactile Guidance System [20]	Precision in alignment and cutting efficiency	Expensive and complex setup	~95%
Laparoscopic Simulation	Visual and vibrotactile feedback [37]	Effective for training novice surgeons	Cognitive overload risk	Not Reported
RMIS Training	Master-slave systems with force reflection [38]	Improved task efficiency and safety	Limited generalizability to all RMIS systems	~85%
Tissue Manipulation	Pneumatic balloon tactile displays [20]	Effective tactile cues in experimental setups	Not widely adopted in clinical settings	Not Reported
Endoscopic Surgery	Sensor integration for grasp force feedback [38]	Improved force control in endoscopic tools	Limited real-world validation	~88%

### 3.3 Methodology

#### 3.3.1 Experimental Setup

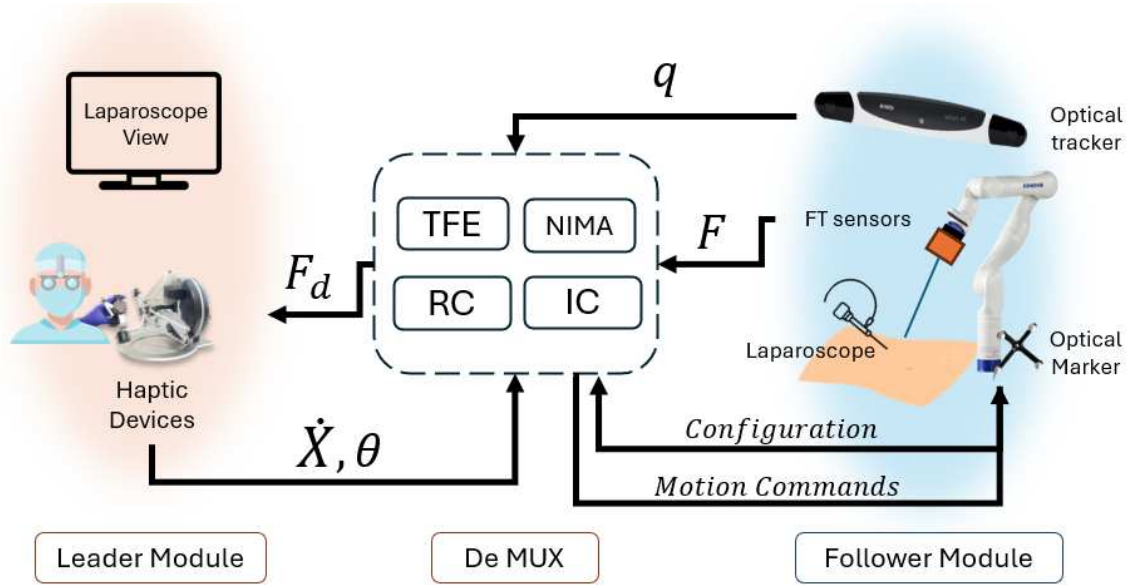


Figure 3.1: System architecture of the presented robot-assisted laparoscopy setup.

The experimental apparatus was carefully designed to simulate a realistic surgical environment, integrating advanced technologies and components, as depicted in Fig. 3.2.

The setup included a custom mannequin embedded with tissue-representative objects, specially designed surgical tools, two Kinova Gen3 robotic arms (7 DOF), dedicated carts for robotic arm stability, two Omega.7 haptic controllers (Force Dimension), three 6-axis force-torque sensors (SenSONE, Bota Systems), and an adaptable, in-house-designed surgical console.

The Kinova Gen3 robotic arms were pivotal for delivering precise and controlled movements of surgical instruments, replicating the dexterity of human hands to ensure an authentic experimental setting for surgical tasks.

Specialized carts were engineered to support the robotic arms, providing stability and flexibility to position the system effectively during experiments.

The surgical tools were custom-designed to integrate seamlessly with the robotic arms while adhering to clinical standards. These tools were powered by four Dynamixel actuators (ROBOTIS),

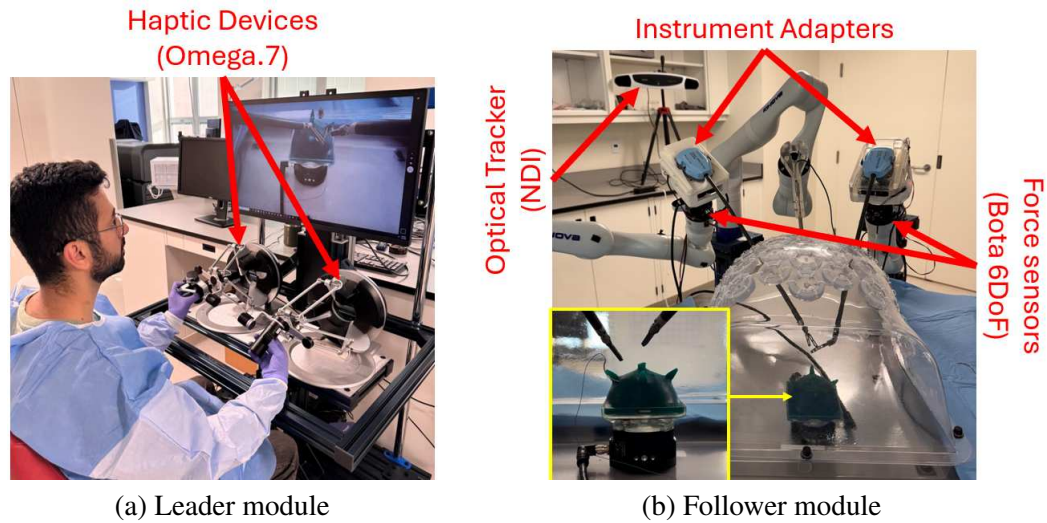


Figure 3.2: a) The developed surgeon’s console with haptic devices. b) The simulated surgical setup, featuring a mannequin, force sensors, an optical tracker, a laparoscope, surgical tools with instrument adapters, and a tissue surrogate.

offering fine-grained control and precision during operations.

The Omega.7 haptic controllers enabled the human operator to intuitively interact with the robotic arms, translating hand movements into precise surgical motions. Their high accuracy played a crucial role in creating realistic and user-friendly surgical simulations.

A translucent mannequin, as shown in Fig. 3.2a, incorporated tissue-representative objects to replicate the structural complexities of real surgical scenarios, including pick-and-place and suturing tasks, fostering an environment that closely mirrors actual surgical challenges.

Force data from simulated tasks were captured using Bota force sensors mounted on the tips of the robotic arms. These sensors provided valuable insights into the mechanical interactions between the surgical tools and the tissue-representative objects.

The custom-designed surgical console, shown in Fig. 3.2b, acted as the central control system, seamlessly integrating the robotic arms, haptic controllers, surgical tools, Dynamixel actuators, and force sensors. This console ensured efficient communication and coordination between all components.

The system architecture, depicted in Fig. 3.1, facilitated control by transmitting commands from the haptic devices to both the Robot Controller (RC) and Instrument Controllers (IC). The robots executed position commands, while the Dynamixel actuators managed the surgical tool tip’s

orientation, with each function handled by a distinct control section. A PID controller was employed for precise position-velocity control, ensuring accurate tooltip alignment.

The robot controller comprised two main modules: one for hand-eye coordination and another for robot communication. It synchronized the robots, optical tracker, laparoscope, and haptic devices with the surgeon's visual perspective for cohesive operation.

Force sensors from Bota, positioned between the robots' end effectors and the custom adapters, measured the interaction forces between the tools and the tissue as well as friction forces at the Remote Center of Motion (RCM). To maintain a stable entry point on the patient's body, translational movements from the surgeon's hand were converted into rotational motions around the RCM. Any friction forces generated during the tool's translational movements were calculated and subtracted from the total forces recorded by the sensors to derive the tooltip forces.

The Tip Force Extractor (TFE) was developed as a neural network block to estimate the tooltip forces using data from the force sensors at the robot's end effectors. This approach, detailed in Section 3.3.4, enabled accurate force calculation for safe and effective haptic feedback. The tool-tissue interaction forces were relayed to the Non-linear Impedance Matching Approach (NIMA) system, which provided adjustable haptic feedback to the surgeon's hands, allowing customization based on the surgeon's preferences.

### 3.3.2 Non-linear Impedance Matching Approach (NIMA)

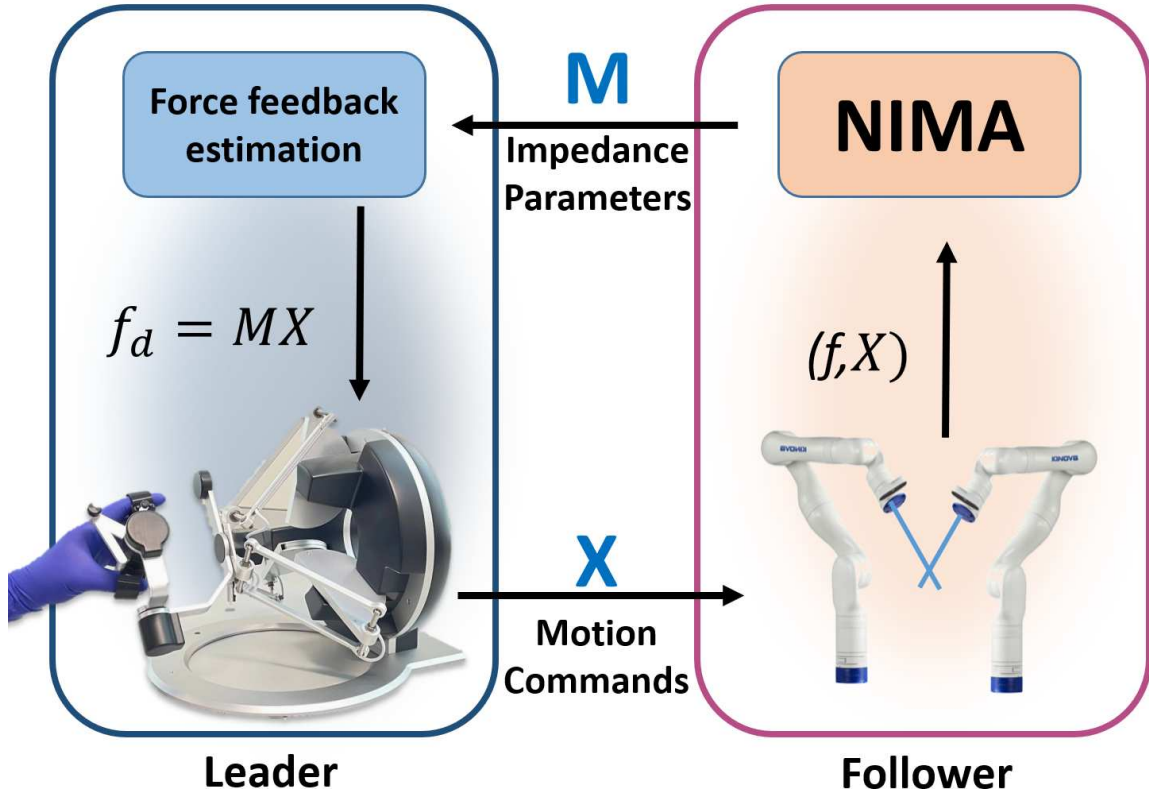


Figure 3.3: The proposed NIMA-based force feedback for haptic-enabled surgical robotics.

This work presents a novel Nonlinear Impedance Matching Approach (NIMA) as an alternative to Direct Force Reflection (DFR) for delivering force feedback in remote surgical robotics. NIMA operates by identifying nonlinear tool-tissue contact impedance parameters, denoted as  $\mathbf{M}$ , at the follower module in real-time and transmitting these parameters to the leader module. Simultaneously, motion commands  $\mathbf{X}$  are sent to the follower module, where a representative laparoscopic tool interacts with a mannequin simulating soft tissue. For simplicity and generality, a polynomial nonlinear impedance model is employed to determine the NIMA parameters  $\mathbf{M}$ . The contact force  $\mathbf{f} \in \mathbb{R}^{3 \times 1}$  is modelled as the response of a nonlinear impedance hyper-surface to the given motion command  $\mathbf{X}$ :

$$\mathbf{f} = \mathbf{M}\mathbf{X} = \mathbf{M} \begin{pmatrix} \mathbf{x}_N^* & \mathbf{y}_N^* & \mathbf{z}_N^* \end{pmatrix}_{1 \times 9N}^T \quad (14)$$

where  $^T$  denotes the transpose operator,  $x$ ,  $y$ , and  $z$  represent the motion commands (i.e., incremental positional changes of the instrument within a time interval  $\delta t$ ), and  $^*_N$  signifies the augmented state operator of degree  $N$ , defined as:

$$\mathbf{u}_N^* = \begin{pmatrix} u & \dot{u} & \ddot{u} & \cdots & u^N & \dot{u}^N & \ddot{u}^N \end{pmatrix}_{3N \times 1} \quad (15)$$

The NIMA impedance parameter matrix  $\mathbf{M}$  is structured as:

$$\mathbf{M} = \begin{pmatrix} \mathbf{m}_x & \mathbf{0} & \mathbf{0} \\ \mathbf{0} & \mathbf{m}_y & \mathbf{0} \\ \mathbf{0} & \mathbf{0} & \mathbf{m}_z \end{pmatrix}_{3 \times 9N} \quad (16)$$

where  $\mathbf{m}_i \in \mathbb{R}^{1 \times 3N}$  is a vector of impedance parameters and  $\mathbf{0} \in \mathbb{R}^{1 \times 3N}$  is a zero vector.

This model assumes no cross-talk between the orthogonal tool-tissue forces along  $x$ ,  $y$ , and  $z$  axes. Cross-talk effects, if needed, can be modelled by including additional non-zero elements in  $\mathbf{M}$ . To compute  $\mathbf{M}$  in real-time, a rolling time window of  $\delta t = 300$  ms was adopted. Delays under 300 ms are generally imperceptible to surgeons in leader-follower setups [35], making this an effective worst-case scenario for updating impedance parameters. The NIMA parameters  $\mathbf{M}$  are continuously updated using a rolling dataset of  $n$  sample forces  $\hat{\mathbf{F}} \in \mathbb{R}^{3 \times n}$  and motion commands  $\hat{\mathbf{X}}$ :

$$\mathbf{M} = \hat{\mathbf{F}} \hat{\mathbf{X}}^+ \quad (17)$$

$$\hat{\mathbf{F}} = \begin{pmatrix} \mathbf{f}_{t_o} & \cdots & \mathbf{f}_{t_o + \delta t} \end{pmatrix}_{3 \times n} \quad (18)$$

$$\hat{\mathbf{X}} = \begin{pmatrix} \mathbf{X}_{t_o} & \cdots & \mathbf{X}_{t_o + \delta t} \end{pmatrix}_{9N \times n} \quad (19)$$

Here,  $\hat{\mathbf{X}}^+$  represents the pseudo-inverse of  $\hat{\mathbf{X}}$ , computed as:

$$\hat{\mathbf{X}}^+ = \hat{\mathbf{X}}^T (\hat{\mathbf{X}} \hat{\mathbf{X}}^T)^{-1} \quad (20)$$

In this research, the peg transfer task, a core element of the Fundamentals of Laparoscopic Surgery (FLS) curriculum [36], was chosen for evaluation. This task involved capturing the robotic arms' positions, orientations, and velocities using two Omega.7 haptic controllers, synchronized to the operator's motion commands at a refresh rate of 1 kHz with a programmed delay of 300 ms. Force feedback, essential for realistic haptic interaction, was recorded via force sensors (SensOne, Bota Systems) at 2 kHz. These data were used to identify NIMA parameters and apply Eq. 14 to compute and render the desired 3D force,  $\mathbf{f}_d$ , on the haptic device. To optimize the polynomial degree  $N$  for NIMA, five parallel threads with  $N = 1 \dots 5$  were executed, with the optimal  $N$  for each time window selected based on minimizing the 3D force reconstruction error. This ensured accurate force feedback and enhanced the surgical simulation's realism.

Despite the validated accuracy of the system in our previous work [19], one critical challenge remains unresolved. Since the force sensor is installed outside the patient's body, the tool-tissue interaction force is not the only contributor to the measured forces. The sensor readings are influenced by additional forces that must be identified and removed before being used as inputs to the Nonlinear Impedance Matching Approach (NIMA).

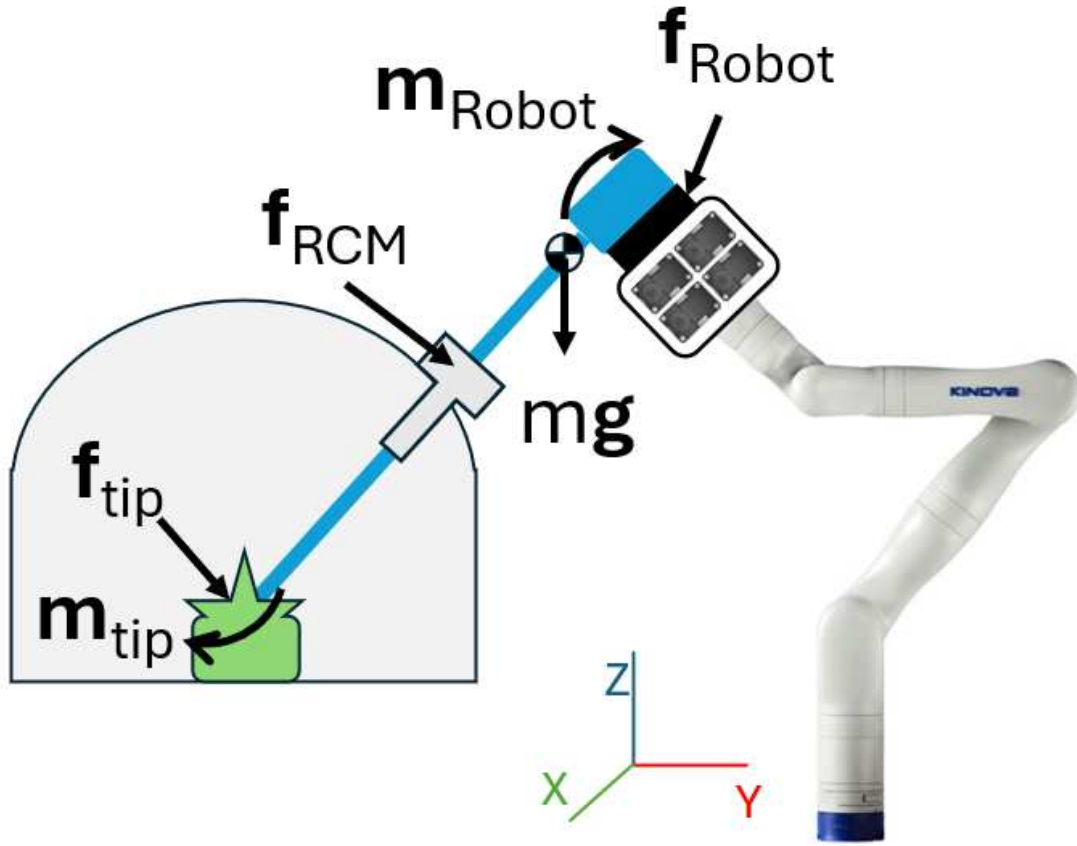


Figure 3.4: Free Body Diagram of the Robotic Laparoscopic Setup During a Typical Task.

Figure 3.4 illustrates the free body diagram of the robotic arm during a task involving interaction between the surgical tool and a tissue surrogate. By assuming a quasi-static motion of the robot's end effector and neglecting inertial forces, the system experiences the following forces:

- Forces measured at the sensor connected to the robotic arm,  $\mathbf{f}_{\text{Robot}}$ ,
- Frictional forces at the Remote Center of Motion (RCM),  $\mathbf{f}_{\text{RCM}}$ ,
- Interaction forces between the tool and tissue,  $\mathbf{f}_{\text{Tip}}$ , and
- Gravitational forces,  $m\mathbf{g}$ .

The equilibrium of forces is given by:

$$\sum \mathbf{F} = \mathbf{f}_{\text{Tip}} + \mathbf{f}_{\text{RCM}} + \mathbf{f}_{\text{Robot}} + m\mathbf{g} = 0 \quad (21)$$

Here,  $\mathbf{f}_{\text{Tip}} \in \mathbb{R}^{3 \times 1}$  represents the interaction forces between the tool and tissue,  $\mathbf{f}_{\text{RCM}} \in \mathbb{R}^{3 \times 1}$  denotes the forces at the RCM,  $\mathbf{f}_{\text{Robot}} \in \mathbb{R}^{3 \times 1}$  refers to the measured forces from the sensor, and  $\mathbf{g} \in \mathbb{R}^{3 \times 1}$  accounts for gravity.

The equilibrium of moments is expressed as:

$$\sum \mathbf{M}_{\text{COM}} = \mathbf{M}_{\text{Robot}} + \mathbf{M}_{f_{\text{Tip}}} + \mathbf{M}_{f_{\text{RCM}}} = 0 \quad (22)$$

where  $\mathbf{M}_{\text{Robot}} \in \mathbb{R}^{3 \times 1}$ ,  $\mathbf{M}_{f_{\text{Tip}}} \in \mathbb{R}^{3 \times 1}$ , and  $\mathbf{M}_{f_{\text{RCM}}} \in \mathbb{R}^{3 \times 1}$  are the moments generated about the Center of Mass (COM) by  $\mathbf{f}_{\text{Robot}}$ ,  $\mathbf{f}_{\text{Tip}}$ , and  $\mathbf{f}_{\text{RCM}}$ , respectively. Substituting the moments using  $\mathbf{r} \times \mathbf{f}$ , the equation becomes:

$$\sum \mathbf{M}_{\text{COM}} = \mathbf{r}_{\text{Robot}} \times \mathbf{F}_{\text{Robot}} + \mathbf{r}_{\text{Tip}} \times \mathbf{F}_{\text{Tip}} + \mathbf{r}_{\text{RCM}} \times \mathbf{f}_{\text{RCM}} = 0 \quad (23)$$

Here,  $\mathbf{r}_{\text{Robot}} \in \mathbb{R}^{3 \times 1}$ ,  $\mathbf{r}_{\text{Tip}} \in \mathbb{R}^{3 \times 1}$ , and  $\mathbf{r}_{\text{RCM}} \in \mathbb{R}^{3 \times 1}$  are the position vectors connecting the respective points to the COM.

From the described forces,  $\mathbf{f}_{\text{Robot}}$  represents the measured forces from the sensor, while  $m\mathbf{g}$  is expressed as:

$$m\mathbf{g} = mg \begin{bmatrix} 0 \\ 0 \\ 1 \end{bmatrix}$$

where  $g$  is the gravitational acceleration. Equations (21) and (23) form a system of equations with  $\mathbf{f}_{\text{Tip}}$  and  $\mathbf{f}_{\text{RCM}}$  as unknowns. On the other hand,  $\mathbf{f}_{\text{Robot}}$ ,  $\mathbf{r}_{\text{Robot}}$ ,  $\mathbf{r}_{\text{Tip}}$ ,  $\mathbf{r}_{\text{RCM}}$ , and  $m\mathbf{g}$  are known, assuming the COM's location is provided. Despite having six equations and six unknowns, an analytical solution is not feasible because two of the equations are redundant. Consequently, a different method is required to determine  $\mathbf{f}_{\text{Tip}}$ .

To address this, a series of experiments were conducted. First, an experiment was designed to eliminate all gravitational forces using a weight compensation method. Subsequently, two additional experiments were conducted to quantify the forces at the RCM and subtract them from the sensor readings, allowing for the accurate determination of tool-tissue interaction forces.

### 3.3.3 Force Sensor Gravity Biasing

For incorporating force feedback into robotic laparoscopic surgery, accurately identifying the force sensor system is essential for applying gravitational biasing, which ensures precise robotic instrument movements. This study employs system identification using IMU data to determine the spatial orientation of the end effector, enabling effective gravitational biasing methods that counteract the effects of gravity on the robotic tools.

To achieve this, IMU sensor Readings were used to calculate the end effector's orientation in real-time without relying on data integration from other sources. Using this IMU data, the system effectively calculates the end effector's roll, pitch, and yaw, critical for compensating gravitational forces acting on the robotic instruments. For simplicity, this method computes roll and pitch angles using accelerations in three directions, avoiding the integration of angular velocity over time [34]. These angles are calculated in real-time through the following equations:

$$\alpha = \text{atan2}(a_y, a_z) \quad (24)$$

$$\beta = \text{atan2}(-a_x, \sqrt{a_y^2 + a_z^2}) \quad (25)$$

Here,  $\alpha$  represents the angle along the world's x-axis,  $\beta$  is the angle along the y-axis, and  $a_x$ ,  $a_y$ , and  $a_z$  are acceleration values along the  $x$ ,  $y$ , and  $z$  directions, respectively.

After deriving the spatial orientation of the end effector from the IMU data, the next step involves modelling gravitational biasing. This model is crucial for implementing techniques to counteract gravity's effects on the robotic tools. The extracted model is expressed as follows:

$$\mathbf{AX} = \mathbf{B} \quad (26)$$

In this equation:

- $\mathbf{A}$  represents the system dynamics,
- $\mathbf{X}$  is the matrix of unknown coefficients,

- $\mathbf{B}$  corresponds to the sensor readings.

The structure of  $\mathbf{A}$  is:

$$\mathbf{A} = \begin{pmatrix} \sin \alpha_{t_1} & \cos \alpha_{t_1} & \sin \beta_{t_1} & \cos \beta_{t_1} & \sin \gamma_{t_1} & \cos \gamma_{t_1} & 1 \\ \sin \alpha_{t_2} & \cos \alpha_{t_2} & \sin \beta_{t_2} & \cos \beta_{t_2} & \sin \gamma_{t_2} & \cos \gamma_{t_2} & 1 \\ \vdots & \vdots & \vdots & \vdots & \vdots & \vdots & \vdots \\ \sin \alpha_{t_n} & \cos \alpha_{t_n} & \sin \beta_{t_n} & \cos \beta_{t_n} & \sin \gamma_{t_n} & \cos \gamma_{t_n} & 1 \end{pmatrix}_{n \times 7} \quad (27)$$

$\mathbf{X}$ , the matrix of unknown coefficients, is defined as:

$$\mathbf{X} = \begin{pmatrix} C_{1x} & C_{1y} & C_{1z} \\ C_{2x} & C_{2y} & C_{2z} \\ C_{3x} & C_{3y} & C_{3z} \\ C_{4x} & C_{4y} & C_{4z} \\ C_{5x} & C_{5y} & C_{5z} \end{pmatrix}_{5 \times 3} \quad (28)$$

Finally,  $\mathbf{B}$ , containing the force readings, is expressed as:

$$\mathbf{B} = \begin{pmatrix} F_{X_{t_1}} & F_{Y_{t_1}} & F_{Z_{t_1}} \\ F_{X_{t_2}} & F_{Y_{t_2}} & F_{Z_{t_2}} \\ \vdots & \vdots & \vdots \\ F_{X_{t_n}} & F_{Y_{t_n}} & F_{Z_{t_n}} \end{pmatrix}_{n \times 3} \quad (29)$$

Here,  $C$  represents the unknown coefficients, and  $F$  denotes the measured forces for a specific robot position.

To determine the coefficient matrix  $\mathbf{X}$ , which is fundamental to the model, the equation  $\mathbf{AX} = \mathbf{B}$  is solved using the pseudo-inverse of  $\mathbf{A}$ :

$$\mathbf{X} = \mathbf{A}^\dagger \mathbf{B} \quad (30)$$

where  $\mathbf{A}^\dagger$  is the pseudo-inverse of  $\mathbf{A}$ , defined as:

$$\mathbf{A}^\dagger = \mathbf{A}^T(\mathbf{A}\mathbf{A}^T)^{-1} \quad (31)$$

Once the coefficient matrix is obtained, the gravitational biasing techniques can be implemented based on the extracted model from the IMU data. These techniques allow robotic instruments to counteract gravitational forces, ensuring precise and reliable movements during laparoscopic surgeries.

### 3.3.4 Tool-tissue Interacting Force Extraction

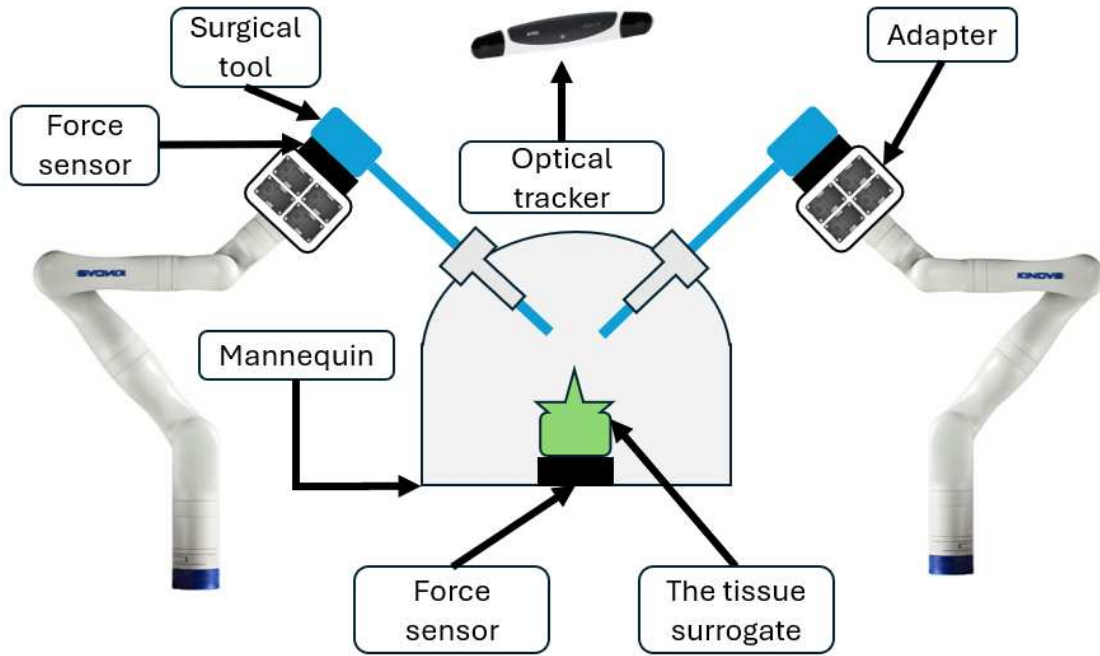


Figure 3.5: The proposed NIMA-based force feedback for haptic-enabled surgical robotics.

After eliminating all gravitational forces due to the weight of the 3D-printed adapter, the tool-tissue forces at the tip of the surgical instrument need to be isolated from the total forces measured by the sensing element. This isolation ensures that only the tool-tip forces are rendered to the surgeon. To achieve this, two experiments were designed to gather data for training a neural network capable of estimating the tool-tip forces solely using force sensors positioned outside the patient's body.

As illustrated in Figure 3.5, the setup for these experiments includes two Bota FT sensors, two

Kinova robotic arms , two instrument adapters, a mannequin, and an NDI optical tracker. Additionally, a silicon-based flexible tissue surrogate, representing human tissue, was mounted on one of the force sensors. These experiments aimed to capture the robotic arm sensor readings, the forces at the tooltip measured via the sensor beneath the flexible tissue surrogate, and the robotic arm end-effector configuration. This data set was subsequently used to train the model.

### Rotation matrices estimation

To use the measured tool-tip forces and those at  $\mathbf{f}_{\text{Robot}}$  for training, both  $\mathbf{f}_{\text{Robot}}$  and  $\mathbf{f}_{\text{Tip}}$  need to be represented within a unified coordinate system. Thus, the first experiment aimed to transform all force readings to the coordinate system of  $\mathbf{f}_{\text{Robot}}$ .

In this experiment, the upper section of the mannequin was removed to eliminate friction forces at the Remote Center of Motion (RCM).

The robotic arm was then manipulated using haptic devices to engage the tool with the tissue surrogate. This setup ensured that the Robot sensor  $S_R$  measured only the interaction forces with the tissue ( $\mathbf{f}_{\text{Robot}}$ ), while the tip sensor  $S_T$  recorded the same forces ( $\mathbf{f}_{\text{Tip}}$ ). Consequently, the forces  $\mathbf{f}_{\text{Tip}}$ , expressed in the coordinate system of  $S_R$ , should match:

$$\{{S_R}\}\mathbf{f}_{\text{Robot}} = \{{S_R}\}\mathbf{f}_{\text{Tip}} \quad (32)$$

where  $\{{S_R}\}\mathbf{f}_{\text{Robot}}$  represents the measured forces of  $S_R$  expressed in its own coordinate system, and  $\{{S_R}\}\mathbf{f}_{\text{Tip}}$  represents the measured forces from  $S_T$  expressed in the coordinate system of  $S_R$ .

Hence:

$$\{{S_R}\}\mathbf{f}_{\text{Robot}} = \{{S_R}\}\mathbf{R}_{\{S_T\}} \{{S_T}\}\mathbf{f}_{\text{Tip}} \quad (33)$$

where the rotation matrix between the coordinate systems can be expressed as:

$$\{{S_R}\}\mathbf{R}_{\{S_T\}} = \{{S_R}\}\mathbf{R}_{\{\text{KBF}\}} \{\text{KBF}\}\mathbf{R}_{\{M\}} \{M\}\mathbf{R}_{\{C\}} \{C\}\mathbf{R}_{\{S_T\}} \quad (34)$$

Here, the coordinate systems are defined as follows:

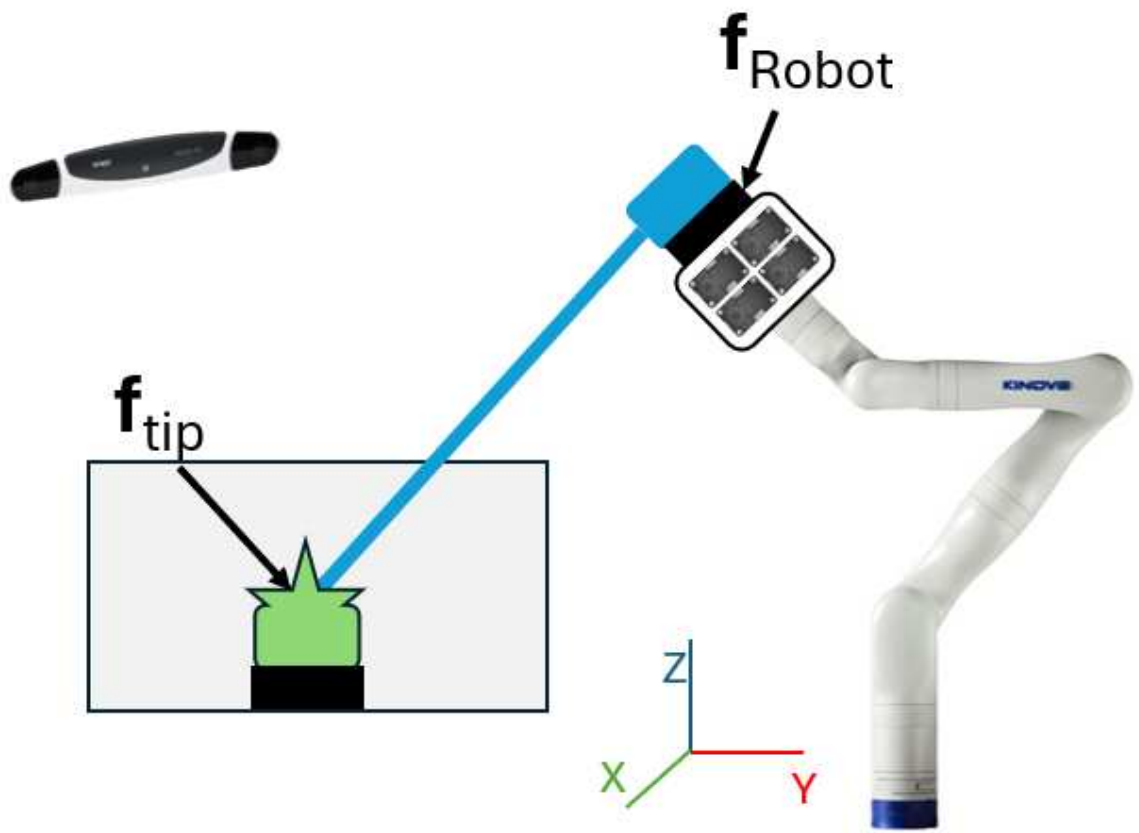


Figure 3.6: Graphical representation of the experimental results demonstrating the relationship between the coordinate systems based on force measurements.

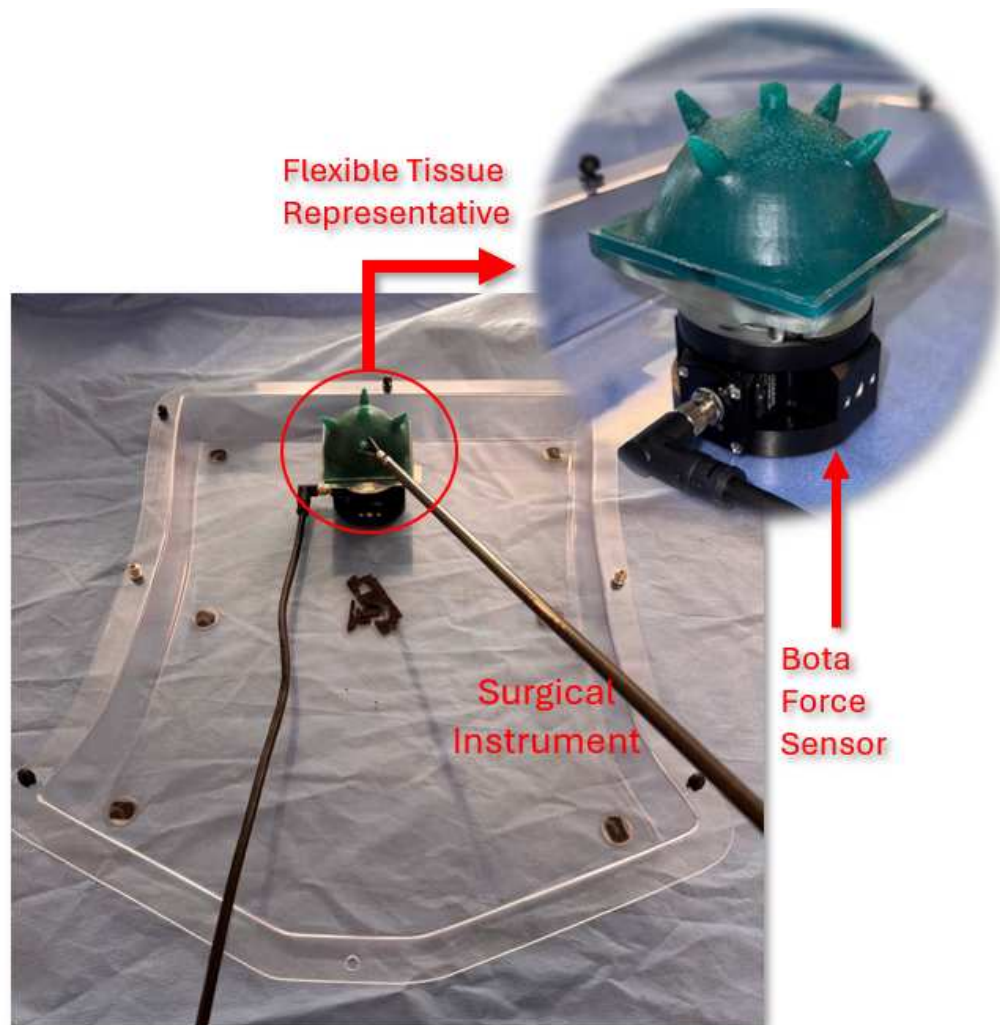


Figure 3.7: Experimental setup for determining the relationship between the coordinate systems. This setup showcases the initial configuration of the robotic arm, tissue surrogate, and force sensors.

- **KBF**: Kinova Base Frame.
- $S_R$ : End effector of the robot holding the instrument.
- **M**: The optical marker attached to the base of the surgical instrument.
- **C**: Optical tracking camera.
- $S_T$ : Coordinate system of the sensor measuring forces at the tip.

In Eq. 34, the only unknown matrix is  ${}^{\{C\}}R_{\{S_T\}}$ , which must be determined. This matrix can be obtained by solving an optimization problem with the objective:

$$\mathbf{R}\mathbf{R}^T = \mathbf{I} \quad (35)$$

subject to the equality constraints:

$$\mathbf{R} = \mathbf{R}_Z(\theta_Z) \mathbf{R}_Y(\theta_Y) \mathbf{R}_X(\theta_X) \quad (36)$$

$${}^{\{S_1\}}\mathbf{R}_{\{C\}} \mathbf{R} {}^{\{S_2\}}\mathbf{F}_t - {}^{\{S_1\}}\mathbf{F}_r = 0 \quad (37)$$

where  $\theta_X$ ,  $\theta_Y$ , and  $\theta_Z$  are the Euler angles along the X, Y, and Z axes, respectively. By optimizing these angles,  ${}^{\{C\}}R_{\{S_T\}}$  can be computed using Eq. 36.

### Neural tip force estimation

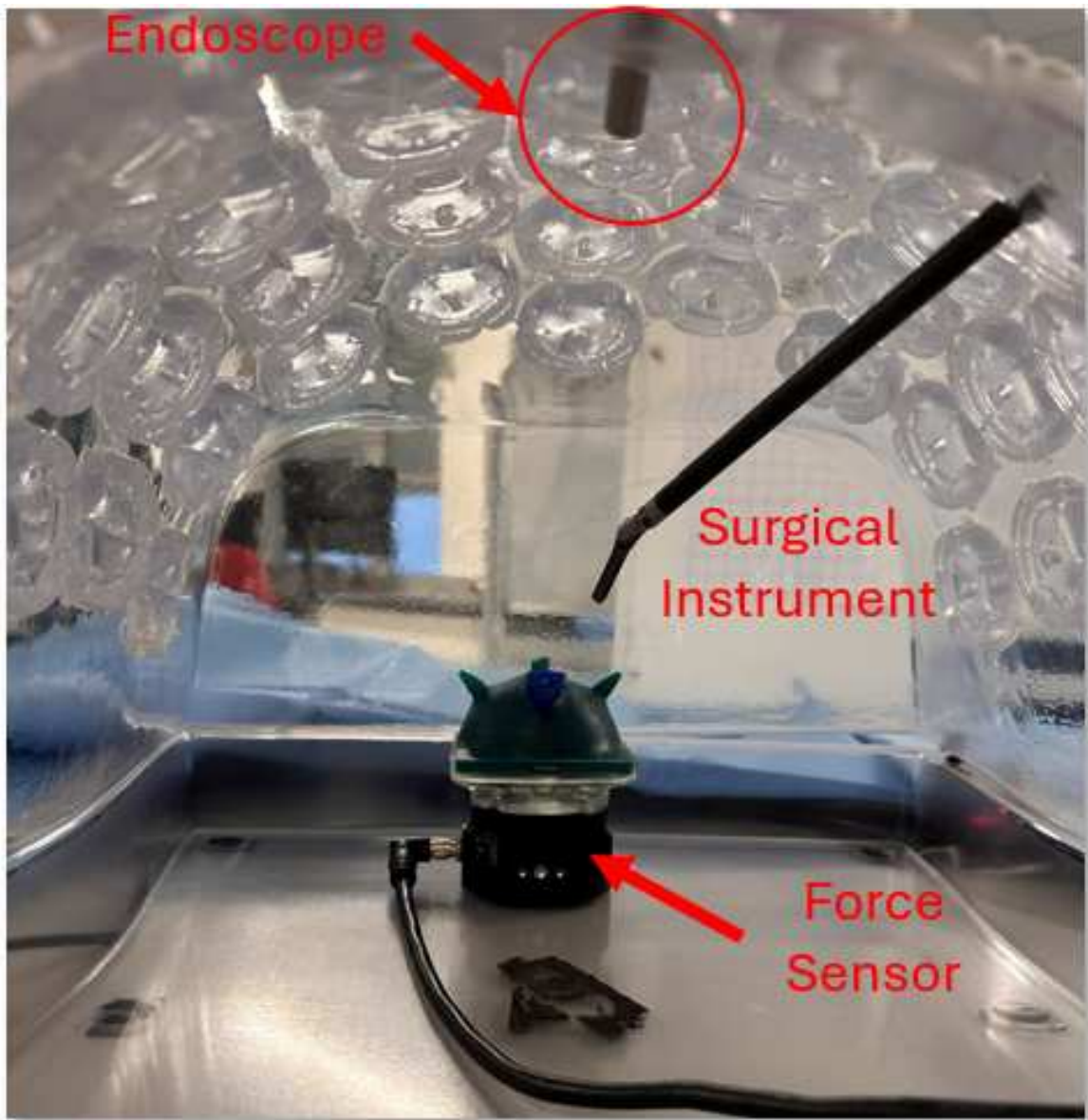


Figure 3.8: An internal view of the mannequin illustrating the setup for Experiment 2. This setup is designed to acquire data for training a neural network to compute tool-tissue interaction forces.

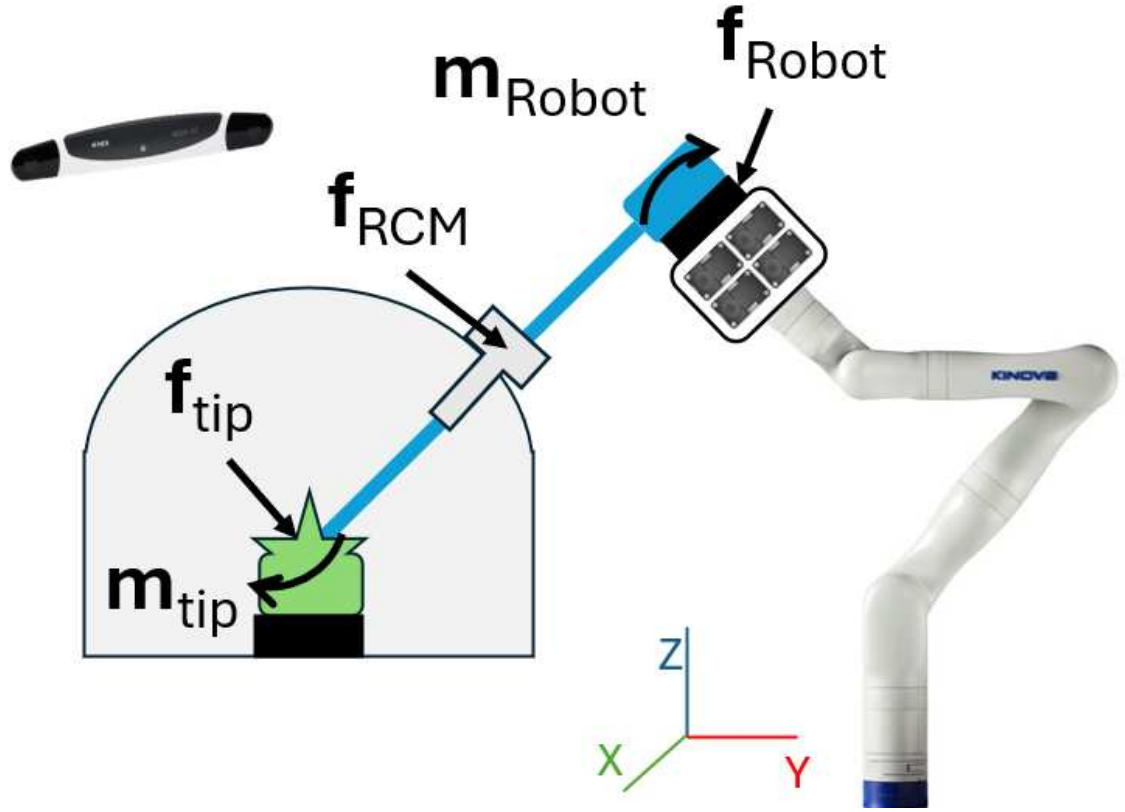


Figure 3.9: The setup for Experiment 2, showing the arrangement of robotic arms, tissue surrogate, and force sensors for capturing tool-tissue interaction data.

Finding the rotation matrix correlations is crucial for expressing all forces with respect to a unified coordinate system. Once that is achieved, the sensor readings can be used to train a neural network to extract the forces at the point of Remote Center of Motion (RCM) and obtain the pure tool tip-tissue interacting forces. To do that, the upper section of the mannequin was installed back on and the same performance was done on the flexible tissue representative covering all the possible movements and configurations of the robot.

By neglecting the inertial forces and considering the movements of the robot to be quasi-static it could be shown that :

$$\sum \mathbf{f} = \mathbf{f}_{\text{Robot}} + \mathbf{f}_{\text{RCM}} + \mathbf{f}_{\text{Tip}} = 0 \quad (38)$$

where  $\mathbf{f}_{\text{Robot}} \in \mathbb{R}^{1 \times 3}$ ,  $\mathbf{f}_{\text{RCM}} \in \mathbb{R}^{1 \times 3}$ , and  $\mathbf{f}_{\text{Tip}} \in \mathbb{R}^{1 \times 3}$  are the forces at the robotic arm,

RCM point, and tip forces. During the experiment,  $\mathbf{f}_{\text{Robot}}, \mathbf{f}_{\text{Tip}}$  and quaternions of the robotic arm  $\mathbf{q}_{\text{Robot}}$  were captured. The dataset used for this study comprised 25,000 samples, each containing predictors  $\mathcal{U}_{\text{Robot}} \in \mathbb{R}^{1 \times 3}$  (robot forces) and  $\mathcal{Q}_{\text{Robot}} \in \mathbb{R}^{1 \times 4}$  (quaternions of the robot's end effector). The responses were  $\mathcal{U}_{\text{Tip}} \in \mathbb{R}^{1 \times 3}$ , representing the tip forces. To ensure a robust evaluation of the model, the dataset was partitioned into three subsets: a training set containing 68% of the data, a validation set with 17%, and a test set comprising the remaining 15%. The training set was used to optimize the model parameters, while the validation set served to monitor the model's performance during training and guide hyperparameter tuning. The test set, which was completely unseen during both training and validation, was reserved to evaluate the final performance of the model and its generalization capability. Before training, the input features were normalized to improve optimization convergence.

The neural network was designed as a fully connected feedforward model. It consisted of an input layer with seven neurons corresponding to the input features, followed by eleven hidden layers, each containing 64 neurons with ReLU activation functions. The output layer included three neurons, reflecting the dimensionality of the target variables, without any activation function, as the task was a regression problem.

The model was compiled using the Mean Squared Error (MSE) as the loss function, which penalizes large prediction errors and is well-suited for regression tasks. The Adam optimizer was employed for its adaptive learning capabilities, ensuring efficient parameter updates throughout training. During the training process, the loss was computed on both the training and validation sets at the end of each epoch. Validation loss indicated the model's ability to generalize to unseen data within the training distribution.

The training and validation loss progression across epochs is depicted in Figure.3.10, highlighting the convergence behaviour and generalization capability of the model. The training procedure spanned 1000 epochs with a batch size of 32. The results showed a Mean Absolute Error (MAE) of 0.1 N, a Maximum Absolute Error (MaxAE) of 0.2 N, and a Root Mean Squared Error (RMSE) of 0.97 N on the test set.

In addition, an additional experiment was designed to evaluate the accuracy and validity of the trained neural network. In this test, the same operation was repeated; however, during this

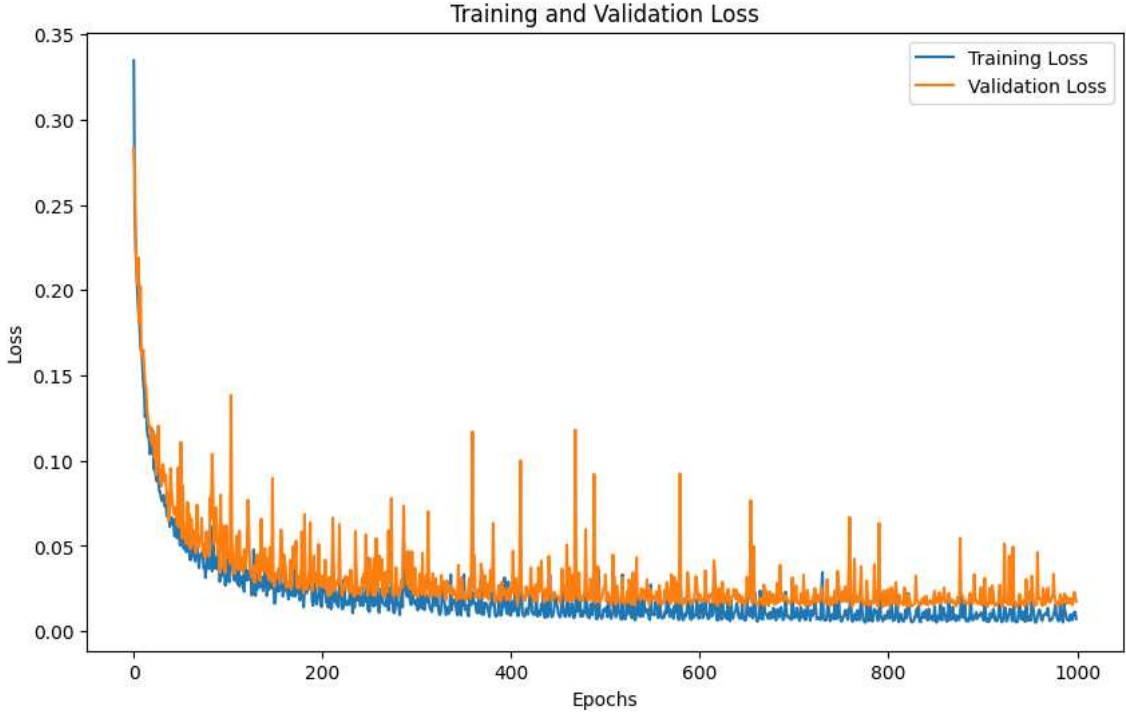


Figure 3.10: Training and validation loss over 1000 epochs, demonstrating convergence and generalization of the neural network model.

procedure, there was no contact between the surgical tool and the tissue. As a result, all the measured  $f_{\text{Tip}}$  values were expected to be zero. Under this condition, the force balance equation simplifies to:

$$\mathbf{f}_{\text{Robot}} = -\mathbf{f}_{\text{RCM}}, \quad (39)$$

indicating that the only forces captured by the robot's force sensor correspond to the forces at the Remote Center of Motion (RCM). Consequently, the prediction of the neural network for the forces at the tooltip should yield zero values, aligning with the experimental setup and verifying the correctness of the model.

### 3.4 Validation Study

The results section is divided into two sections: results of the Experiment 3.3.4 and the results indicating the effectiveness of the presented NIMA model.

### Results of the Experiment 3.3.4

The results of the first experiment are presented in Fig. 3.4, which illustrates the tool-tissue interaction forces captured by two force sensors with respect to the KBF. This data validates the calibration method used to establish the relationship between the coordinate systems.

A comparative analysis between the forces measured by the sensor attached to the robotic arm and those measured by the tissue surrogate's sensor reveals a Mean Absolute Error (MAE) of 0.11 N, 0.09 N, and 0.13 N in the  $X$ ,  $Y$ , and  $Z$  directions respectively. The Standard Deviations (SD) for these measurements are 0.11 N, 0.12 N, and 0.18 N, respectively, demonstrating the precision of the calibration.

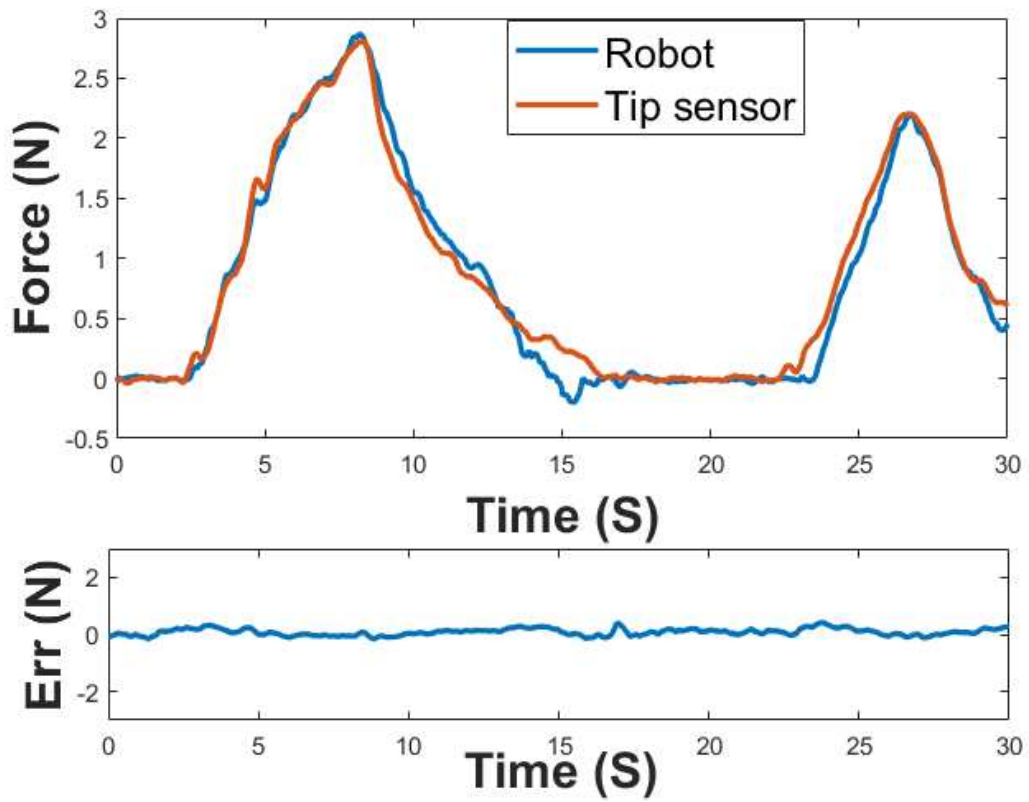
Figure 3.13 demonstrates the results of the trained neural network (NN) model in subtracting friction forces to isolate the tip forces applied by the surgical tool. The comparative analysis in the  $X$ ,  $Y$ , and  $Z$  directions highlights the accuracy of this model in extracting the tip forces.

The Mean Absolute Error (MAE) between the measured and predicted forces for the  $X$ ,  $Y$ , and  $Z$  axes are  $0.19 \pm 0.2$  N,  $0.16 \pm 0.2$  N, and  $0.16 \pm 0.2$  N respectively. A statistical analysis further confirms the model's effectiveness, showing the predicted forces fall within the 95% confidence interval.

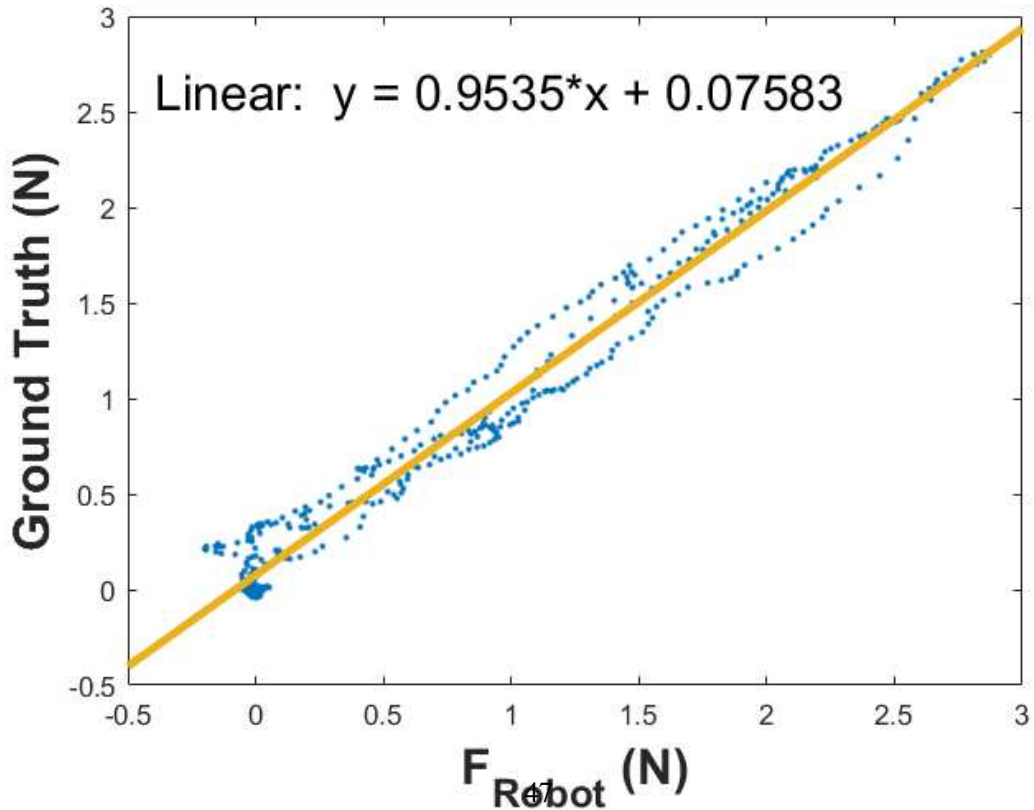
Figures 3.14, 3.15, and 3.16 show the results of an extra experiment where there was no contact between the surgical tool and the tissue representative and the only captured forces were frictional forces at the point of RCM. The measured forces in this experiment are the forces captured by the untouched sensor which only captured the noise from the sensor. However, the NN model performed beyond that and captured forces with an even lower range of error than the force sensor. The mae values for the predicted forces are  $0.02 \pm 0.03$  N,  $0.02 \pm 0.03$  N, and  $0.02 \pm 0.03$  N in the  $X$ ,  $Y$ , and  $Z$  directions respectively. Moreover, the distribution of the forces in one of the axes is demonstrated in fig 3.17 solidifying the results mentioned.

### Results of NIMA

The effectiveness of our Nonlinear Impedance Matching Approach (NIMA) in accurately rendering forces on haptic devices is illustrated in Fig. 3.18.



(a) Forces in the Y direction with respect to KBR



(b) Force comparison in the Y direction

Figure 3.11: Illustration of the forces in the Y direction: (a) forces in the Y direction with respect

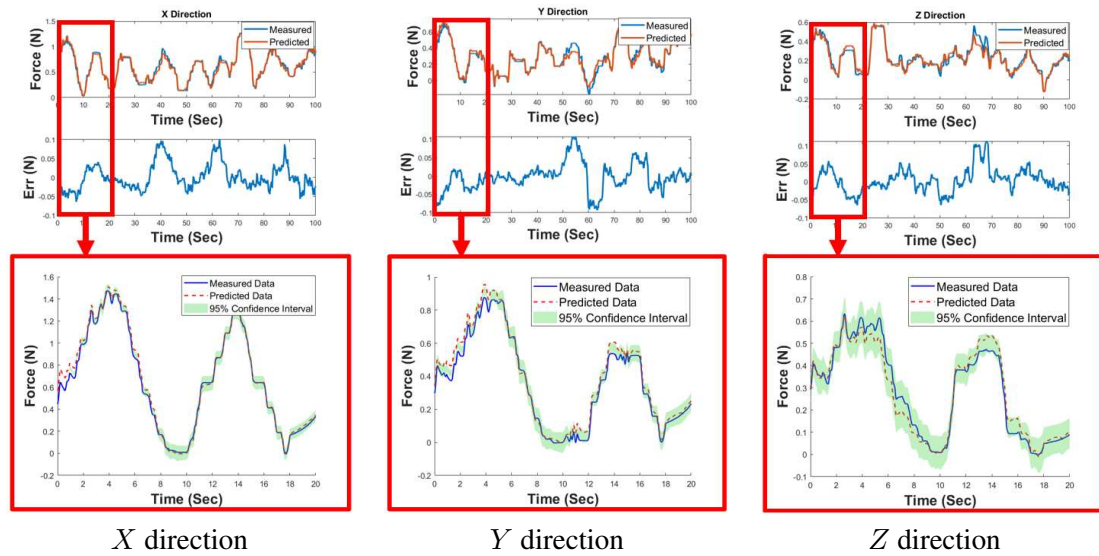


Figure 3.12: Illustration of the model's performance in the  $X$ ,  $Y$ , and  $Z$  directions.

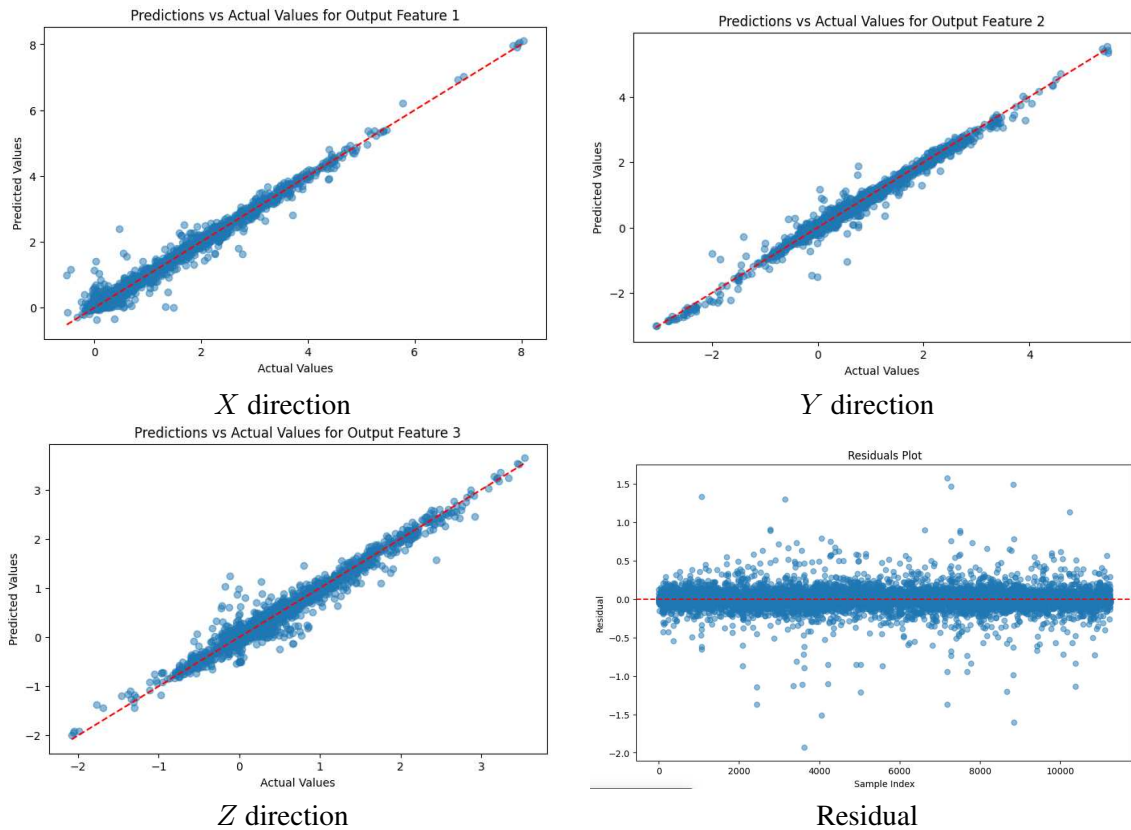


Figure 3.13: Illustration of the trained neural network (NN) model's performance in extracting tip forces along the (a)  $X$ , (b)  $Y$ , and (c)  $Z$  directions, and (d) the residuals, highlighting its accuracy and statistical reliability.

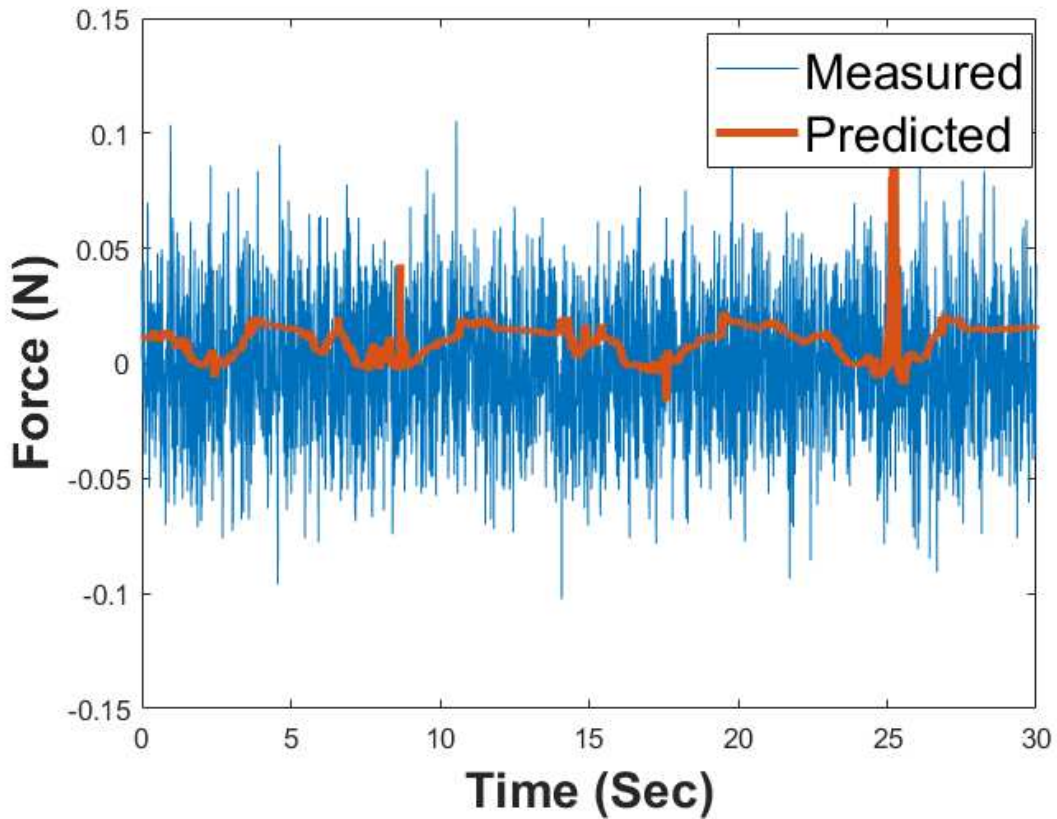


Figure 3.14: Accuracy of the neural network (NN) model in capturing and subtracting frictional forces at the Remote Center of Motion (RCM) in the  $X$  direction, enabling precise extraction of tip forces for force rendering.

Figure 3.18 compares the forces rendered by the haptic device to the actual forces measured by force sensors. The implementation of NIMA achieved a Mean Absolute Error (MAE) of 0.01 N, demonstrating high fidelity in force feedback. The errors followed a normal distribution with a Standard Deviation (SD) of 0.02 N. This performance significantly exceeds that of the Linear Impedance Matching Approach (IMA), which recorded an MAE of 0.2 N and an SD of 0.4 N.

A comparative assessment reveals a 95% improvement in accuracy with NIMA. This enhancement underscores the superior precision of the nonlinear approach in generating force feedback, setting a new benchmark for realism and immersion in haptic interactions. The substantial reduction in MAE highlights the effectiveness of integrating nonlinear dynamics into impedance-matching processes, improving both the quality and reliability of haptic feedback.

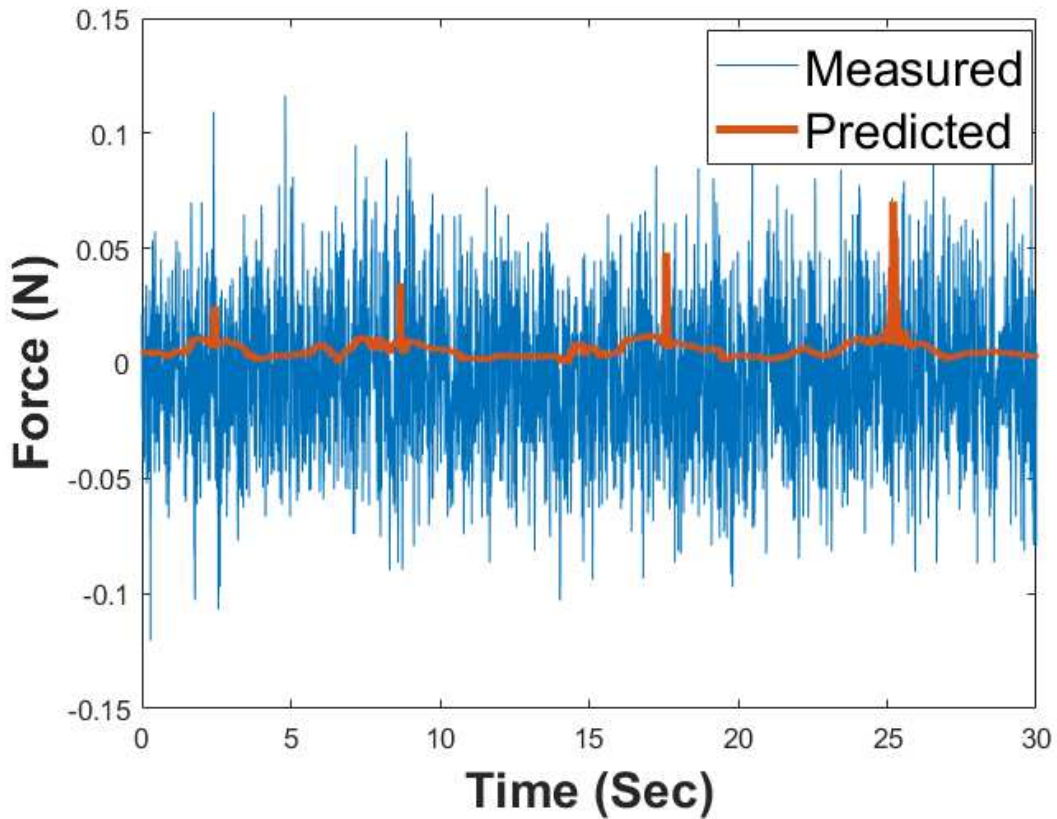


Figure 3.15: Accuracy of the neural network (NN) model in capturing and subtracting frictional forces at the Remote Center of Motion (RCM) in the  $Y$  direction, enabling precise extraction of tip forces for force rendering.

Furthermore, Fig. 3.18 demonstrates how NIMA addresses the kick-back behaviour by rendering no forces for movements with velocities below 1 mm/s. Consequently, when the user releases the haptic device, no force is applied to the handles, ensuring they remain stationary. However, resisting forces are rendered with high accuracy once user input exceeds the velocity threshold, preserving NIMA's precision.

A detailed analysis of the algorithm's performance throughout the experiment revealed a noteworthy preference for nonlinear models, with a nonlinear fit being selected in over 64% of the evaluated time windows. This reliance on nonlinear approaches highlights the limitations of the Linear Impedance Matching (IMA) model in capturing the intricate, dynamic interactions between surgical tools and tissue. The complexity and variability of these interactions exceed the representational capabilities of linear models, emphasizing the nuanced nature of tool-tissue forces encountered during

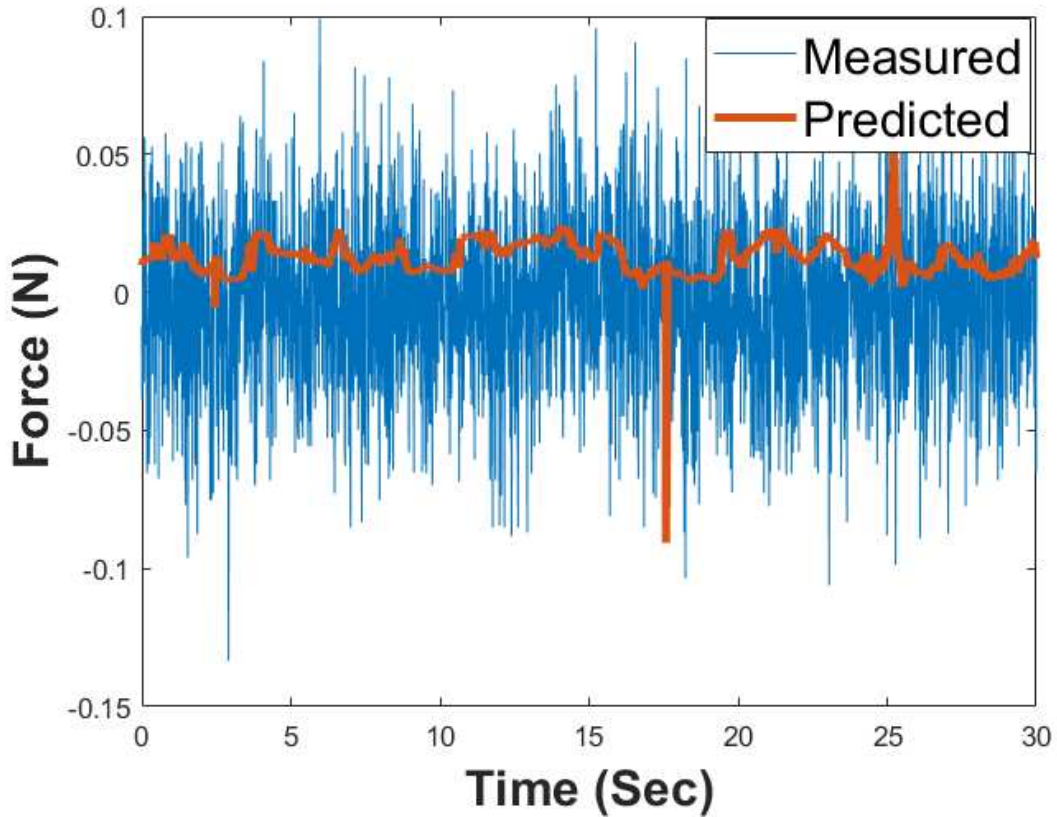


Figure 3.16: Accuracy of the neural network (NN) model in capturing and subtracting frictional forces at the Remote Center of Motion (RCM) in the  $Z$  direction, enabling precise extraction of tip forces for force rendering.

laparoscopic procedures. These findings suggest that temporal variations in these forces—crucial for realistic haptic feedback—are better captured through nonlinear modelling, enabling a more accurate and responsive simulation of surgical scenarios.

### 3.5 Discussions

Throughout our experiments, the phenomenon commonly referred to as "haptic kick" — a sudden, unwelcome jerk felt by the operator upon the release of the haptic device — was notably absent. This observation is consistent with the mechanisms we have previously described [33], wherein the rapid convergence of the system's output force vector,  $\mathbf{X}$ , to zero within a brief time window,  $\delta t$ , upon the user releasing the haptic device ensures that the desired force,  $\mathbf{f}_d$ , also approaches zero.

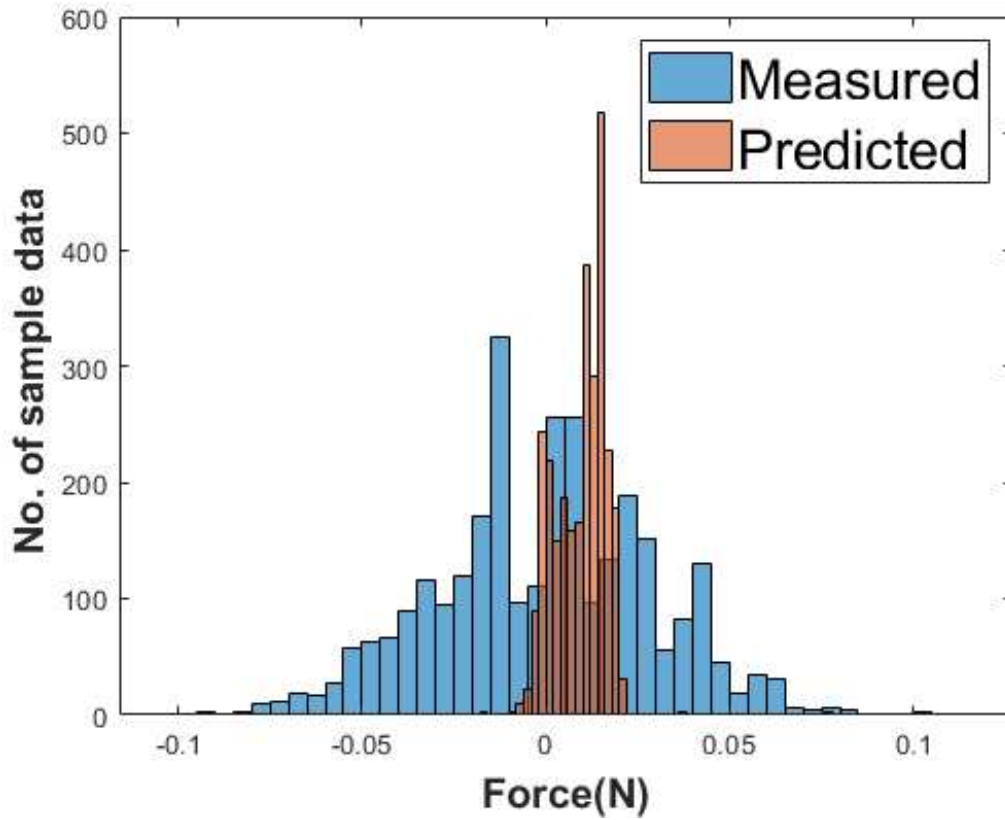


Figure 3.17: A histogram illustrating the effectiveness of the neural network (NN) model in accurately capturing forces at the Remote Center of Motion (RCM), facilitating the precise extraction of tool-tissue interaction forces.

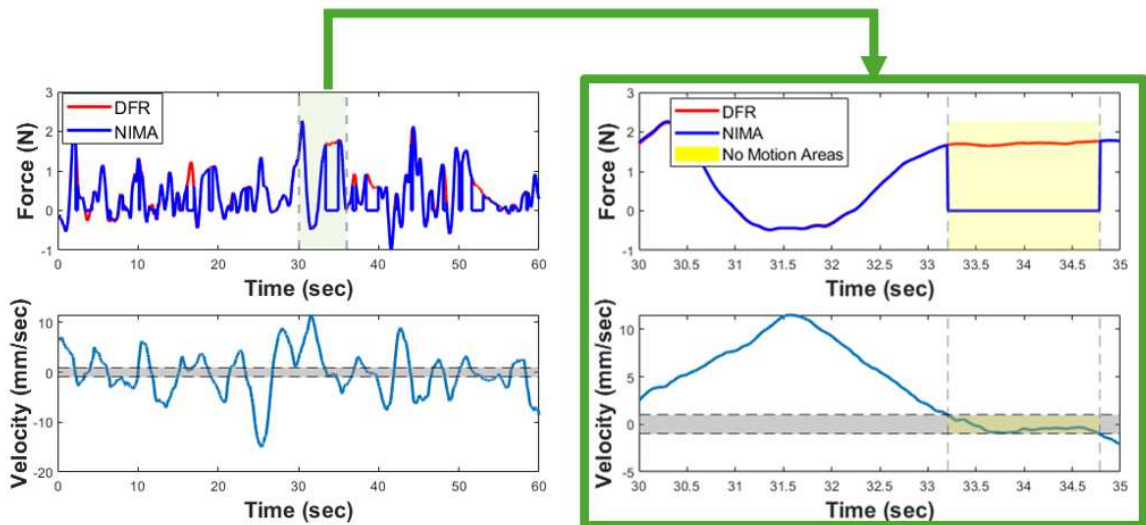


Figure 3.18: A comparison between the rendered force using NIMA and the measured force with DFR as the ground truth.

This behaviour effectively neutralizes the potential for a haptic kickback, thereby enhancing the safety and comfort of the operator's experience. The elimination of the haptic kick in our system not only improves user interaction with the haptic device but also represents a significant step forward in the development of more sophisticated and user-friendly haptic feedback systems for surgical training simulators.

### **3.6 Summary**

The Nonlinear Impedance Matching Approach (NIMA) presented in this study represents a significant advancement in the development of haptic feedback systems for robot-assisted surgery. By leveraging a nonlinear impedance model, NIMA effectively captures the complex dynamics of tool-tissue interactions, enabling precise control of 3D contact forces and enhancing the realism of haptic feedback. The experimental results underscore its superior accuracy and stability compared to linear impedance methods, demonstrating an 85% improvement in force rendering fidelity and successfully eliminating undesirable phenomena such as haptic kickback.

NIMA's ability to accurately replicate surgical forces without destabilizing the system offers a transformative solution to one of the major limitations of existing teleoperated surgical systems. Furthermore, the method's adaptability to dynamic and nonlinear conditions highlights its potential for broader application across various surgical scenarios and robotic platforms. These findings pave the way for integrating haptic feedback into commercial robotic surgical systems, thereby addressing a critical gap in the field and enhancing both the safety and efficacy of minimally invasive procedures.

As robotic surgery continues to advance, the development and adoption of robust haptic systems like NIMA will play a crucial role in improving surgical training, optimizing clinical outcomes, and ultimately setting new standards for precision and reliability in robotic-assisted medical interventions.

## Chapter 4

# Conclusion and Future Works

### 4.1 Conclusions

In this research, the Nonlinear Impedance Matching Approach (NIMA) was introduced to address the critical challenges of force rendering in robotic-assisted laparoscopic surgery. First, the design requirements for a robust haptic feedback system were identified, including the need to accurately replicate tool-tissue interaction forces within an error margin of less than 10

To meet these design requirements and avoid introducing additional complexities to the surgical workflow, a novel haptic rendering methodology was developed. The NIMA framework incorporates nonlinear dynamics to improve force fidelity and system responsiveness while maintaining intrinsic safety. Unlike traditional methods, NIMA was designed to eliminate haptic kickback, ensuring that no force is applied to the haptic device when the surgeon releases the handle. This innovation enhances both user comfort and patient safety.

A neural network-based tool-tissue force estimation method was developed as part of this research, enabling accurate extraction of interaction forces from externally placed force sensors. The neural model compensated for extraneous forces, such as friction at the Remote Center of Motion (RCM) and gravitational effects, achieving a mean absolute error (MAE) of 0.01 N. This force estimation method met the accuracy requirements set in the research objectives and provided a foundation for high-fidelity haptic feedback.

To validate the NIMA framework, an experimental setup was designed and implemented, featuring commercially available robotic arms, haptic controllers, and custom-designed surgical tools. The results demonstrated a significant improvement in force rendering fidelity, achieving a 95

The proposed framework also includes a roadmap for future advancements, such as extending NIMA into torque feedback channels and integrating it with physics-informed neural network (PINN) models for self-supervised, model-free force rendering. These extensions would further enhance the adaptability and scalability of the system.

In addition, the validated experimental setup confirmed the compatibility of the developed components, including force estimation, haptic rendering, and rotation measurement, with the overall system design requirements. The integrated system demonstrated stability, precision, and scalability, addressing the longstanding need for realistic and reliable haptic feedback in robotic-assisted surgical systems.

Based on the presented contributions and performance evaluations, this research establishes NIMA as a feasible and transformative technology for addressing the unmet need for haptic feedback in minimally invasive surgery. The proposed system not only advances the state of the art in robotic surgery but also paves the way for broader applications in medical robotics and training simulators.

## **4.2 Future Works**

Building upon the advancements achieved in this research, several avenues for future work have been identified to further enhance the capabilities and applications of the Nonlinear Impedance Matching Approach (NIMA) in robotic-assisted surgery:

- (1) **Integration of Torque Feedback:** While this research focused on force rendering, extending NIMA to incorporate torque feedback would provide surgeons with a more comprehensive tactile experience. This addition would enable precise control of rotational forces, further improving the realism and utility of haptic feedback in robotic-assisted laparoscopic procedures.
- (2) **Development of a Physics-Informed Neural Network (PINN):** The integration of NIMA with a physics-informed neural network (PINN) model could enable self-supervised, model-free

force rendering. This approach would eliminate the need for predefined tissue models, allowing the system to adapt to a wide variety of surgical scenarios dynamically and autonomously.

- (3) **Structural Optimization for Zero-Force Rendering:** Although the proposed haptic rendering modality demonstrated the feasibility of generating zero force, structural optimization of the prototyped system is necessary to achieve this capability consistently. Future work should focus on refining the design and materials used in the haptic rendering system to enhance performance and reliability.
- (4) **Extension to Multi-DOF Systems:** Expanding the framework to include additional degrees of freedom (DOF) for both force and torque rendering would enhance its applicability to more complex surgical tasks, such as those requiring simultaneous manipulation and suturing.
- (5) **Integration with Commercial Robotic Systems:** While the current research utilized custom experimental setups, integrating NIMA into commercially available robotic platforms, such as the da Vinci Surgical System, would facilitate its adoption in clinical settings. Collaboration with industry partners could expedite this process.
- (6) **Real-Time Applications and Clinical Trials:** Although the system demonstrated high fidelity and safety in experimental conditions, future research should focus on optimizing computational efficiency to enable real-time applications. Conducting clinical trials will also be essential to validate the system's performance in real-world surgical scenarios and ensure its compliance with medical regulatory standards.
- (7) **Surgeon Training and Feedback:** Developing training modules for surgeons to familiarize them with NIMA-based haptic feedback systems could improve adoption and usability. Gathering detailed feedback from surgeons during trials will inform iterative improvements to the system design.
- (8) **Exploration of New Surgical Applications:** Beyond laparoscopic surgery, NIMA could be adapted for other minimally invasive surgical domains, such as neurosurgery or endovascular interventions. This adaptation would involve customizing the force and torque rendering parameters to meet the specific requirements of these procedures.

By addressing these future directions, the NIMA framework can continue to evolve as a cutting-edge solution for enhancing haptic feedback in robotic surgery. These advancements will not only improve surgical precision and patient outcomes but also establish a new standard for the integration of haptics in robotic-assisted medical interventions.

# Bibliography

- [1] Kuo Chen, Narasimha M Beeraka, Jin Zhang, . . . , Mikhail Y. Sinelnikov, and Liudmila M. Mikhaleva. Efficacy of da vinci robot-assisted lymph node surgery than conventional axillary lymph node dissection in breast cancer – a comparative study. *International Journal of Medical Robotics and Computer Assisted Surgery*, 2021. doi: 10.1002/rcs.2307.
- [2] Ioannis D. Gkegkes, Ioannis Mamais, and Christos Iavazzo. Robotics in general surgery: A systematic cost assessment. *Journal of Minimal Access Surgery*, 2017. doi: 10.4103/0972-9941.195565.
- [3] Youn-Jee Chung, So Yeon Kang, Mi Rang Choi, Hyun Hee Cho, Jang Heub Kim, and Mee-Ran Kim. Robot-assisted laparoscopic adenomyomectomy for patients who want to preserve fertility. *Yonsei Medical Journal*, 2016. doi: 10.3349/ymj.2016.57.6.1531.
- [4] Benjamin B. Albright, Tilman Witte, Alena N. Tofte, Jeremy Chou, Jonathan Black, Vrunda B. Desai, and Elisabeth A. Erekson. Robotic versus laparoscopic hysterectomy for benign disease: A systematic review and meta-analysis of randomized trials. *Journal of Minimally Invasive Gynecology*, 2016. doi: 10.1016/j.jmig.2015.08.003.
- [5] Estefanía Ruiz Guerrero, A.V. Ojeda Claro, M.J. Ledo Cepero, M. Soto Delgado, and José Luís Fernández. Robotic versus laparoscopic partial nephrectomy in the new era: Systematic review. *Cancers*, 2023. doi: 10.3390/cancers15061793.
- [6] AI Ikebuchi. Outcome of robot-assisted surgery for stage ia endometrial cancer compared to open and laparoscopic surgery: A retrospective study at a single institution. 2023. doi: 10.21203/rs.3.rs-3728184/v1.

- [7] Inci Sahin and Bilgi Baca. Robotic-assisted laparoscopic complete mesocolic excision. *Digestive Disease Interventions*, 2023. doi: 10.1055/s-0042-1760369.
- [8] Sehyun Baek, Dong Hoon Lee, and Seon Hahn Kim. Current status of robot-assisted gastric surgery. *World Journal of Gastrointestinal Oncology*, 2011. doi: 10.4251/wjgo.v3.i10.137.
- [9] Longke Ran, Jing Jin, Yan Xu, Youquan Bu, and Fangzhou Song. Comparison of robotic surgery with laparoscopy and laparotomy for treatment of endometrial cancer: A meta-analysis. *Plos One*, 2014. doi: 10.1371/journal.pone.0108361.
- [10] Y. He, Y. Zhang, and X. Liu. The role of haptic feedback in robotic-assisted surgery: A review. *International Journal of Medical Robotics and Computer Assisted Surgery*, 9(3):275–283, 2013. doi: 10.1002/ircs.1515.
- [11] H. Wu, L. Chen, and Y. Zhao. Mechanical properties of biological tissues: Implications for robotic surgery. *Biomechanics and Modeling in Mechanobiology*, 21(3):789–802, 2022. doi: 10.1007/s10237-021-01412-4.
- [12] J. Ueda. Advances in haptic technology for robotic surgery: Current trends and future directions. *Surgical Innovation*, 30(1):45–52, 2023. doi: 10.1177/15533506211012345.
- [13] J. Currie, A. Smith, and R. Johnson. The impact of haptic feedback on surgical performance: A systematic review. *Journal of Robotic Surgery*, 10(4):345–352, 2016. doi: 10.1007/s11701-016-0623-4.
- [14] J. Zhu, Z. Liu, and Y. Chen. The limitations of visual feedback in robotic surgery: A review of the literature. *Surgical Endoscopy*, 30(5):2030–2036, 2016. doi: 10.1007/s00464-015-4315-5.
- [15] I. Farkhatdinov and J. Ryu. Control issues in robotic systems with force feedback: Implications for surgical applications. *International Journal of Robotics Research*, 29(6):749–762, 2010. doi: 10.1177/0278364909356683.
- [16] A. Abiri, M. Parnian, and M. Khosravi. The impact of haptic feedback on surgical precision: A review of current literature. *Journal of Robotic Surgery*, 13(1):1–10, 2019. doi: 10.1007/s11701-018-0810-5.

- [17] J. R. Bethea, T. J. Smith, and L. A. Johnson. The effects of haptic feedback on surgical performance: A clinical study. *Surgical Endoscopy*, 18(4):654–658, 2004. doi: 10.1007/s00464-003-9035-8.
- [18] M. Rehan, A. Othman, and M. Khan. Real-time force feedback systems in robotic surgery: Challenges and opportunities. *Medical Image Analysis*, 73:102–115, 2022. doi: 10.1016/j.media.2021.102115.
- [19] Aiden Mazidi, Andrés C Ramos, Amir Sayadi, Javad Dargahi, Jake Barralet, Liane S Feldman, and Amir Hooshier. Nonlinear impedance matching approach (nima) for robust haptic rendering during robotic laparoscopy surgery. In *2024 10th IEEE RAS/EMBS International Conference for Biomedical Robotics and Biomechatronics (BioRob)*, pages 1809–1814. IEEE, 2024.
- [20] F. Amirabdollahian, S. Livatino, B. Vahedi, R. Gudipati, P. Sheen, S. Gawrie-Mohan, and N. Vasdev. Prevalence of haptic feedback in robot-mediated surgery: a systematic review of literature. *Journal of Robotic Surgery*, 12:11–25, 2017. doi: 10.1007/s11701-017-0763-4.
- [21] A. M. Okamura. Methods for haptic feedback in teleoperated robot-assisted surgery. *Industrial Robot: An International Journal*, 31:499–508, 2004. doi: 10.1108/01439910410566362.
- [22] C. Pacchierotti, D. Prattichizzo, and K. J. Kuchenbecker. Cutaneous feedback of fingertip deformation and vibration for palpation in robotic surgery. *IEEE Transactions on Biomedical Engineering*, 63:278–287, 2016. doi: 10.1109/tbme.2015.2455932.
- [23] O. v. d. Meijden and M. P. Schijven. The value of haptic feedback in conventional and robot-assisted minimal invasive surgery and virtual reality training: a current review. *Surgical Endoscopy*, 23:1180–1190, 2009. doi: 10.1007/s00464-008-0298-x.
- [24] A. A. Gumbs, I. Frigerio, G. Spolverato, R. S. Croner, A. Illanes, E. Chouillard, and E. Elyan. Artificial intelligence surgery: how do we get to autonomous actions in surgery? *Sensors*, 21:5526, 2021. doi: 10.3390/s21165526.

- [25] Amir Hooshier, Siamak Najarian, and Javad Dargahi. Haptic telerobotic cardiovascular intervention: a review of approaches, methods, and future perspectives. *IEEE reviews in biomedical engineering*, 13:32–50, 2019.
- [26] M. Zhou, Y. Qi-ming, K. Huang, S. Mahov, A. Eslami, M. Maier, C. P. Lohmann, N. Navab, D. Zapp, A. Knoll, and M. A. Nasser. Towards robotic-assisted subretinal injection: a hybrid parallel–serial robot system design and preliminary evaluation. *IEEE Transactions on Industrial Electronics*, 67:6617–6628, 2020. doi: 10.1109/tie.2019.2937041.
- [27] M. J. Fu and M. C. Çavuşoğlu. Human-arm-and-hand-dynamic model with variability analyses for a stylus-based haptic interface. *IEEE Transactions on Systems, Man, and Cybernetics, Part B (Cybernetics)*, 42:1633–1644, 2012. doi: 10.1109/tsmcb.2012.2197387.
- [28] D. Prattichizzo, C. Pacchierotti, and G. Rosati. Cutaneous force feedback as a sensory subtraction technique in haptics. *IEEE Transactions on Haptics*, 5:289–300, 2012. doi: 10.1109/toh.2012.15.
- [29] B. Siciliano. Parallel force/position control of robot manipulators. *Robotics Research*, pages 78–89, 1996. doi: 10.1007/978-1-4471-1021-7\_9.
- [30] S. S. Parsi, M. V. Sivaselvan, and A. S. Whittaker. Impedance-matching model-in-the-loop simulation. *Earthquake Engineering & Structural Dynamics*, 52:3600–3621, 2023. doi: 10.1002/eqe.3922.
- [31] Z. Pezzementi, E. Plaku, C. Reyda, and G. D. Hager. Tactile-object recognition from appearance information. *IEEE Transactions on Robotics*, 27:473–487, 2011. doi: 10.1109/tro.2011.2125350.
- [32] G. Liu, Y. Wang, C. Huang, C. Guan, D. Ma, Z. Wei, and X. Qiu. Experimental evaluation on haptic feedback accuracy by using two self-made haptic devices and one additional interface in robotic teleoperation. *Actuators*, 11:24, 2022. doi: 10.3390/act11010024.
- [33] Amir Sayadi, Amir Hooshier, and Javad Dargahi. Impedance matching approach for robust

- force feedback rendering with application in robot-assisted interventions. In *2020 8th International Conference on Control, Mechatronics and Automation (ICCMA)*, pages 18–22. IEEE, 2020.
- [34] Amir Hooshidar, Amir Sayadi, Javad Dargahi, and Siamak Najarian. Integral-free spatial orientation estimation method and wearable rotation measurement device for robot-assisted catheter intervention. *IEEE/ASME Transactions on Mechatronics*, 27(2):766–776, 2022. doi: 10.1109/TMECH.2021.3071295.
- [35] M. Perez, F. Quiaios, P. Andrivon, D. Husson, M. Dufaut, J. Felblinger, and J. Hubert. Paradigms and experimental set-up for the determination of the acceptable delay in telesurgery. *2007 29th Annual International Conference of the IEEE Engineering in Medicine and Biology Society*, 2007. doi: 10.1109/iembs.2007.4352321.
- [36] G. M. Fried. Fls assessment of competency using simulated laparoscopic tasks. *Journal of Gastrointestinal Surgery*, 12:210–212, 2007. doi: 10.1007/s11605-007-0355-0.
- [37] J. Colan, A. Davila, and Y. Hasegawa. A review on tactile displays for conventional laparoscopic surgery. *Surgeries*, 3(4):334–346, 2022. doi: 10.3390/surgeries3040036.
- [38] Amir Hadi Hosseinabadi and Septimiu E. Salcudean. Force sensing in robot-assisted keyhole endoscopy: A systematic survey. *The International Journal of Robotics Research*, 41(2):136–162, 2021. doi: 10.1177/02783649211052067.
- [39] Allison M. Okamura, Lisa N. Verner, Carol E. Reiley, and Mohsen Mahvash. Haptics for robot-assisted minimally invasive surgery. In *Springer Tracts in Advanced Robotics*, pages 361–373. Springer, Berlin, Heidelberg, 2010. doi: 10.1007/978-3-642-14743-2\\_30.

Appendix

## .1 Appendix

The following components were designed, fabricated in-house, and used in the robot-assisted laparoscopic system developed for this research:

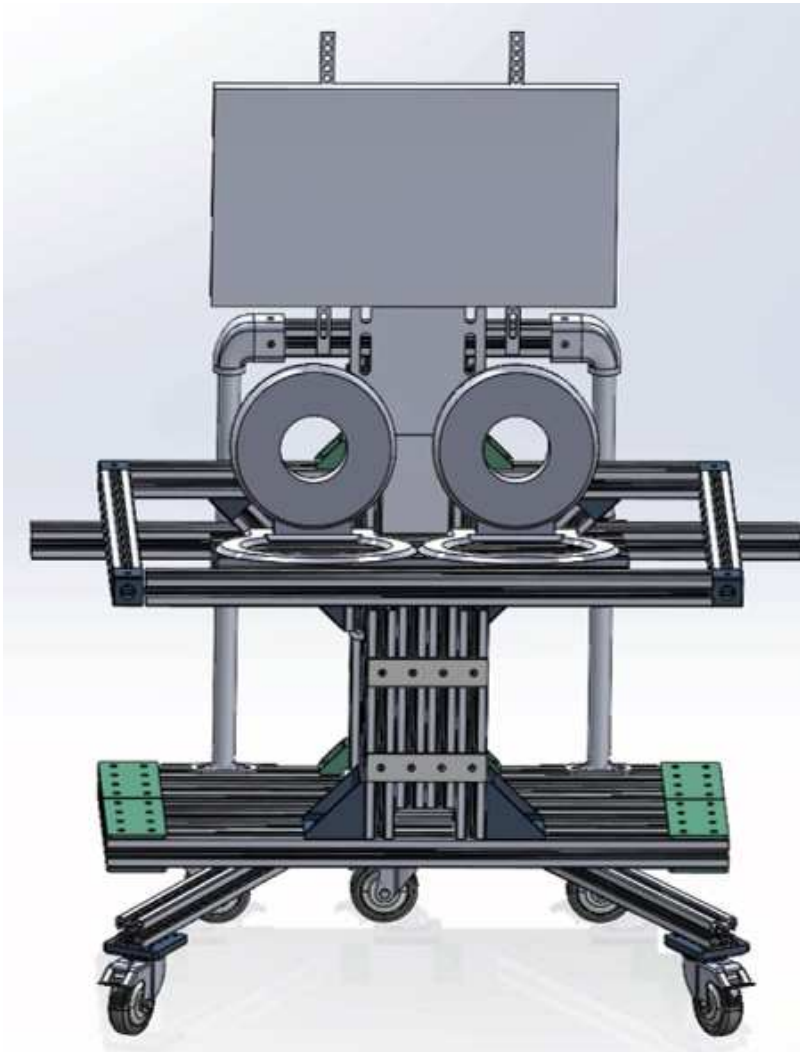


Figure .1: Design of the surgeon console used in the robot-assisted laparoscopic system developed to in this research.



Figure .2: The surgeon console designed, assembled, and used in the robot-assisted laparoscopic system developed in this research.



Figure .3: The Adapter designed, 3D printed in-house, and used in the Follower Module: Integration with 4 Dynamixel Motors as the Main Actuation Unit for Surgical Tool Control.



Figure .4: The laparoscope holder designed, fabricated, and used in the Follower Module: a flange to connect the laparoscope to Kinova robotic arms.

### **Programming Scripts**

```
WeightR1 = vecnorm(Fr1,2,2);
```

WeightR2 = vecnorm(Fr2,2,2);

WeightR3 = vecnorm(Fr3,2,2);

WeightR4 = vecnorm(Fr4,2,2);

WeightR5 = vecnorm(Fr5,2,2);

a = 1.341;

b = 0.005577;

$WeightR_{Correct1} = a * WeightR1 + b;$

$WeightR_{Correct2} = a * WeightR2 + b;$

$WeightR_{Correct3} = a * WeightR3 + b;$

$WeightR_{Correct4} = a * WeightR4 + b;$

$WeightR_{Correct5} = a * WeightR5 + b;$

$Fr_{Corrected1} = (Fr1./WeightR1). * WeightR_{Correct1};$

$Fr_{Corrected2} = (Fr2./WeightR2). * WeightR_{Correct2};$

$Fr_{Corrected3} = (Fr3./WeightR3). * WeightR_{Correct3};$

$Fr_{Corrected4} = (Fr4./WeightR4). * WeightR_{Correct4};$

$Fr_{Corrected5} = (Fr5./WeightR5). * WeightR_{Correct5};$

*for* i = 1 : length(FrCorrected1)

$Fr_{Corrected_{wrtC1}}(i, 1 : 3) = T1(4 * i - 3 : 4 * i - 1, 1 : 3) * RS1 * Fr_{Corrected1}(i, 1 : 3)';$

$Fr2(i, 1 : 3) = TC2(4 * i - 3 : 4 * i - 1, 1 : 3) * RP * Fr_{Corrected2}(i, 1 : 3)';$

$FrC3(i, 1 : 3) = T3(4 * i - 3 : 4 * i - 1, 1 : 3) * RP * Fr_{Corrected3}(i, 1 : 3)';$

end

*for*  $i = 1 : \text{length}(Ft1)$

$Ft_{wrtC1}(i, 1 : 3) = RC * Ft1(i, 1 : 3)'$ ;

$Ft_{wrtC2}(i, 1 : 3) = RC * Ft2(i, 1 : 3)'$ ;

$Ft_{wrtC3}(i, 1 : 3) = RC * Ft3(i, 1 : 3)'$ ;

**end**

*for*  $i = 1 : \text{length}(Ft1)$

$Quaternions1(i, 1 : 4) = \text{rotationMatrixToQuaternion}(TC1(4 * i - 3 : 4 * i - 1, 1 : 3))$ ;

$Quaternions2(i, 1 : 4) = \text{rotationMatrixToQuaternion}(TC2(4 * i - 3 : 4 * i - 1, 1 : 3))$ ;

$Quaternions3(i, 1 : 4) = \text{rotationMatrixToQuaternion}(TC3(4 * i - 3 : 4 * i - 1, 1 : 3))$ ;

$X1(i) = TC1(4 * i - 3, 4)$ ;

$Y1(i) = TC1(4 * i - 2, 4)$ ;

$Z1(i) = TC1(4 * i - 1, 4)$ ;

$X2(i) = TC2(4 * i - 3, 4)$ ;

$Y2(i) = TC2(4 * i - 2, 4)$ ;

$Z2(i) = TC2(4 * i - 1, 4)$ ;

$X3(i) = TC3(4 * i - 3, 4)$ ;

$Y3(i) = TC3(4 * i - 2, 4)$ ;

$Z3(i) = TC3(4 * i - 1, 4)$ ;

**end**

*for*  $i = 1 : \text{length}(Quaternions1) - 1$

$i\text{fabs}(Quaternions1(i + 1, 1) - Quaternions1(i, 1)) > 0.1$

$Quaternions1(i + 1, 1) = -Quaternions1(i + 1, 1);$

end

$ifabs(Quaternions1(i + 1, 2) - Quaternions1(i, 2)) > 0.1$

$Quaternions1(i + 1, 2) = -Quaternions1(i + 1, 2);$

end

$ifabs(Quaternions1(i + 1, 3) - Quaternions1(i, 3)) > 0.1$

$Quaternions1(i + 1, 3) = -Quaternions1(i + 1, 3);$

end

$ifabs(Quaternions1(i + 1, 4) - Quaternions1(i, 4)) > 0.1$

$Quaternions1(i + 1, 4) = -Quaternions1(i + 1, 4);$

end

end

$for i = 1 : length(Quaternions2) - 1$

$ifabs(Quaternions2(i + 1, 1) - Quaternions2(i, 1)) > 0.1$

$Quaternions2(i + 1, 1) = -Quaternions2(i + 1, 1);$

end

$ifabs(Quaternions2(i + 1, 2) - Quaternions2(i, 2)) > 0.1$

$Quaternions2(i + 1, 2) = -Quaternions2(i + 1, 2);$

end

$ifabs(Quaternions2(i + 1, 3) - Quaternions2(i, 3)) > 0.1$

$Quaternions2(i + 1, 3) = -Quaternions2(i + 1, 3);$

end

$ifabs(Quaternions2(i + 1, 4) - Quaternions2(i, 4)) > 0.1$

$Quaternions2(i + 1, 4) = -Quaternions2(i + 1, 4);$

end

end

$for i = 1 : length(Quaternions3) - 1$

$ifabs(Quaternions3(i + 1, 1) - Quaternions3(i, 1)) > 0.1$

$Quaternions3(i + 1, 1) = -Quaternions3(i + 1, 1);$

end

$ifabs(Quaternions3(i + 1, 2) - Quaternions3(i, 2)) > 0.1$

$Quaternions3(i + 1, 2) = -Quaternions3(i + 1, 2);$

end

$ifabs(Quaternions3(i + 1, 3) - Quaternions3(i, 3)) > 0.1$

$Quaternions3(i + 1, 3) = -Quaternions3(i + 1, 3);$

end

*ifabs(Quaternions3(i + 1, 4) - Quaternions3(i, 4)) > 0.1*

*Quaternions3(i + 1, 4) = -Quaternions3(i + 1, 4);*

*end*

*end*

*Predictors = [FrCorrected\_wrtC1, Quaternions1;*

*FrCorrected\_wrtC2, Quaternions2;*

*FrCorrected\_wrtC3, Quaternions3];*

*Responses = [Ft\_wrtC1; Ft\_wrtC2; Ft\_wrtC3];*

*total\_rows = 30000;*

*num\_split = 25000;*

*random\_indices = randperm(total\_rows, num\_split);*

*Predictors\_25000\_Rand = Predictors(random\_indices, :); Responses\_25000\_Rand = Responses(random\_indices, :);*

*remaining\_indices = setdiff(1 : total\_rows, random\_indices);*

*Predictors\_5000\_Rand = Predictors(remaining\_indices, :);*

*Responses\_5000\_Rand = Responses(remaining\_indices, :);*

*writematrix(Predictors\_25000\_Rand, 'Predictors\_25000\_Rand.csv');*

*writematrix(Predictors\_5000\_Rand, 'Predictors\_5000\_Rand.csv');*

*writematrix(Responses\_25000\_Rand, 'Responses\_25000\_Rand.csv');*

*writematrix(Responses\_5000\_Rand, 'Responses\_5000\_Rand.csv');*

```

MyModel = load("MyTipForceExtractionNNModel.mat");
FtPredicted5000Rand = MyModel.MyTipForceExtractionNNModel.Network(Predictors5000Rand');

Measured_dataX = movmean(Responses5000Rand(1 : 1000, 1), 200);
Measured_dataY = movmean(Responses5000Rand(1 : 1000, 2), 200);
Measured_dataZ = movmean(Responses5000Rand(1 : 1000, 3), 200);
Predicted_DataX = movmean(FtPredicted5000Rand(1 : 1000, 1), 200);
Predicted_DataY = movmean(FtPredicted5000Rand(1 : 1000, 2), 200);
Predicted_DataZ = movmean(FtPredicted5000Rand(1 : 1000, 3), 200);
errorX = Measured_dataX - Predicted_DataX;
errorY = Measured_dataY - Predicted_DataY;
errorZ = Measured_dataZ - Predicted_DataZ;

SigmaX = 1.4826 * mad(errorX, 1);
SigmaY = 1.4826 * mad(errorY, 1);
SigmaZ = 1.4826 * mad(errorZ, 1);

upper_boundX = Measured_dataX + 2 * SigmaX;
lower_boundX = Predicted_DataX - 2 * SigmaX;

upper_boundY = Measured_dataY + 2 * SigmaY;
lower_boundY = Predicted_DataY - 2 * SigmaY;

upper_boundZ = Measured_dataZ + 2 * SigmaZ;
lower_boundZ = Predicted_DataZ - 2 * SigmaZ;

figure;
hold on;

```

```

t1 = linspace(0, 20, length(PredictedDataX));
plot(t1, MeasuredDataX, 'b-', 'LineWidth', 1.5, 'DisplayName', 'MeasuredData');

plot(t1, PredictedDataX, 'r--', 'LineWidth', 1.5, 'DisplayName', 'PredictedData');

```

```

legend show;
xlabel('Time (Sec)');
ylabel('Force (N)');
title('Measured Data with  $\pm 2\sigma$  Bounds X axis');
hold off;

```

```

figure;
hold on;

```

```

plot(t1, MeasuredDataY, 'b-', 'LineWidth', 1.5, 'DisplayName', 'MeasuredData');

plot(t1, PredictedDataY, 'r--', 'LineWidth', 1.5, 'DisplayName', 'PredictedData');

```

```

    xlabel('Time (Sec)');
ylabel('Force (N)');
title('Measured Data with  $\pm 2\sigma$  Bounds Y axis');
hold off;

```

```

figure;
hold on;

```

```

plot(t1, MeasuredDataZ, 'b-', 'LineWidth', 1.5, 'DisplayName', 'MeasuredData');

```

```

    plot(t1, PredictedDataZ, 'r - -', 'LineWidth', 1.5, 'DisplayName', 'PredictedData');

    legendshow;
xlabel('Time(Sec)');
ylabel('Force(N)');
title('MeasuredData with  $\pm 2\sigma$  Bounds Z axis');
hold off;

    t2 = linspace(0, 100, length(FtPredicted5000Rand(:, 1)));
figure
subplot(2,1,1)
plot(t2, movmean(Responses5000Rand(:, 1), 300));
hold on;
plot(t2, movmean(FtPredicted5000Rand(:, 1), 300));
xlabel("Time(Sec)")
ylabel("Force(N)")
legend("Measured", "Predicted")
title("X Direction")
hold off
subplot(2, 1, 2)
plot(t2, movmean(Responses5000Rand(:, 1) - FtPredicted5000Rand(:, 1), 300))
xlabel("Time(Sec)")
ylabel("Err(N)")

figure
subplot(2,1,1)
plot(t2, movmean(Responses5000Rand(:, 2), 300));
hold on;

```

```

plot(t2, movmean(FtPredicted5000Rand(:, 2), 300));
xlabel("Time(Sec)")
ylabel("Force(N)")
legend("Measured", "Predicted")
title("Y Direction")
hold off
subplot(2, 1, 2)
plot(t2, movmean(Responses5000Rand(:, 2) - FtPredicted5000Rand(:, 2), 300))
xlabel("Time(Sec)")
ylabel("Err(N)")

```

```

figure
subplot(2, 1, 1)
plot(t2, movmean(Responses5000Rand(:, 3), 300));
hold on;
plot(t2, movmean(FtPredicted5000Rand(:, 3), 300));
xlabel("Time(Sec)")
ylabel("Force(N)")
legend("Measured", "Predicted")
title("Z Direction")
hold off
subplot(2, 1, 2)
plot(t2, movmean(Responses5000Rand(:, 3) - FtPredicted5000Rand(:, 3), 300))
xlabel("Time(Sec)")
ylabel("Err(N)")

```

```

MAEX = mae(Responses5000Rand(:, 1) - FtPredicted5000Rand(:, 1));
MAEY = mae(Responses5000Rand(:, 2) - FtPredicted5000Rand(:, 2));
MAEZ = mae(Responses5000Rand(:, 3) - FtPredicted5000Rand(:, 3));

```

```
 $STD_X = std(Responses_{5000}Rand(:, 1) - Ft_{Predicted}_{5000}Rand(:, 1));$   
 $STD_Y = std(Responses_{5000}Rand(:, 2) - Ft_{Predicted}_{5000}Rand(:, 2));$   
 $STD_Z = std(Responses_{5000}Rand(:, 3) - Ft_{Predicted}_{5000}Rand(:, 3));$ 
```

```
clc;  
 $disp('mae_X :'); disp(MAE_X);$   
 $disp('mae_Y :'); disp(MAE_Y);$   
 $disp('mae_Z :'); disp(MAE_Z);$ 
```

```
 $disp('std_X :'); disp(STD_X);$   
 $disp('std_Y :'); disp(STD_Y);$   
 $disp('std_Z :'); disp(STD_Z);$ 
```